TABLE 2. Characteristics of Six Lines of Tg Rabbits

Line	Site of Insertion	Estimated Copy Number	Ratio of Transgene to Endogenous Opsin mRNA	Amplitude of Maximum Scotopic ERG a-Wave at 12 Wk (μV)
7	13q	30	4:1	49.6 ± 12.7 (n = 5)
8	12q	10	1:1	96.5 ± 20.1 (n = 5)
10	2q	1	0.15:1	180.2 (n = 1)
11	Xq	3	0.07:1	165.1 (n = 1)
14	9p	3	0.1:1	159.3 (n = 1)
16*	6q, 3p	Variable	Variable	Variable

Maximum scotopic ERGs (mixed rod and cone response) were measured with high intensity flash stimulus of 2.2 log cd · s · m^{-2}. Results are expressed as the mean ± SD. The a-wave amplitude of WT NZW rabbits was 170 ± 28 μV (n = 5).

* Double copy line.

chromosomes that yielded two different lines, 16a and 16b (Fig. 2B).

The transgene copy number estimated by Southern blot analysis correlated roughly with the level of transgene expression and the degree of photoreceptor degeneration as determined by the ERG a-wave amplitude (Table 2). Lines 7 and 8, which had higher transgene copy numbers, had higher levels of transgene expression and showed a rapid, progressive reduction in the a-wave amplitude. In contrast, lines 10, 11, and 14, which had lower copy numbers, had lower transgene expression levels, and the a-wave amplitude was not significantly different from that of age-matched (12 weeks of age) WT rabbits. The a-wave amplitudes for these three lines remained within the normal range, even at 48 weeks (data not shown).

Because of a restriction in the number of rabbits that could be housed in our animal facilities, we mainly produced and investigated line 7, which had the highest level of transgene expression and the most severe photoreceptor degeneration.

Clinical Findings

Tg rabbits from all lines had normal corneas, anterior chambers, and clear lenses. There was no difference in the fundus appearance or fluorescein angiograms between WT and Tg rabbits at any age up to 40 weeks (Fig. 3). However, it should be noted that Tg animals were on an albino background, and the characteristic bone spicule pigmentation of the retina seen in RP eyes would therefore not be expected.

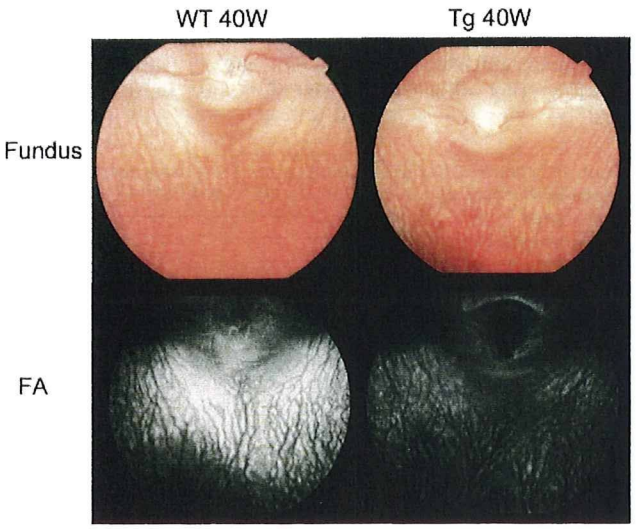

FIGURE 3. Fundus photographs (*top*) and fluorescein angiograms (*bottom*) obtained from a 40-week-old WT and a rhodopsin P347L Tg rabbit from line 7. The appearances of the fundus and the angiogram of the Tg rabbit were indistinguishable from those of the WT rabbit, even at 40 weeks.

Retinal Histology and Immunohistochemistry

Retinal histology in the area of the visual streak, the central area of the rabbit retina, of a WT and a line 7 Tg rabbit at different ages are shown in Figure 4A. At 2 weeks of age, the retinal histology of Tg rabbits was nearly indistinguishable from that of WT rabbits. Both types of rabbits had six or seven layers of nuclei in the ONL. Thereafter, the thickness of the ONL in Tg rabbits progressively decreased (Fig. 4B). At 48 weeks, only a single row of nuclei remained in the ONL of the retina of Tg rabbits. In contrast, the architecture and thickness of the middle and inner retinal layers were relatively well preserved even at 48 weeks of age.

We also examined the retina of Tg rabbits by immunohistochemistry using an anti-rhodopsin antibody and PNA lectin. There was no detectable rhodopsin labeling in the retina of 48-week-old Tg rabbit in the area of the visual streak (Fig. 5). The cone inner and outer segments were stained by PNA, but their structures were severely disrupted in the 48-week-old Tg rabbit.

There were distinct regional differences in the degree of photoreceptor loss in the older Tg rabbits. The retinal sections from 12-week-old WT and Tg rabbits at three locations along the vertical meridian are shown in Figure 4C. It is known that in normal rabbits, the density of rod and cone photoreceptors is highest at the visual streak located inferior to the optic nerve head.[20] Consistent with previous reports, the thickness of the ONL in WT rabbits was at its maximum near the visual streak. In contrast, the ONL in Tg rabbits was thinnest near the visual streak and was relatively preserved in the peripheral retina (Fig. 4D).

ERGs of Tg Rabbits

To evaluate the retinal function of the rod and cone systems of Tg rabbits, we recorded full-field scotopic and photopic ERGs. The scotopic and photopic ERGs elicited by different stimulus intensities from a 12-week-old WT and 12- and 48-week-old Tg rabbits are shown in Figures 6A and 6B, respectively. Compared with the ERGs recorded from 12-week-old WT rabbits, the ERG amplitudes of Tg rabbits were clearly reduced at 12 weeks, and the degree of reduction became more severe at 48 weeks. The amplitude of the maximum rod a-wave, which reflects rod photoreceptor activity, was 28% of the WT at 12 weeks and reduced to 5% at 48 weeks (Fig. 6C). In contrast, the maximum cone a-wave amplitude was 65% of the WT at 12 weeks and remained at 35% even at 48 weeks (Fig. 6D). The a-wave fitting model of Hood and Birch[28] also revealed that not only the maximum response amplitude (Rm), but also the transduction sensitivity (S) were abnormal in both rod and

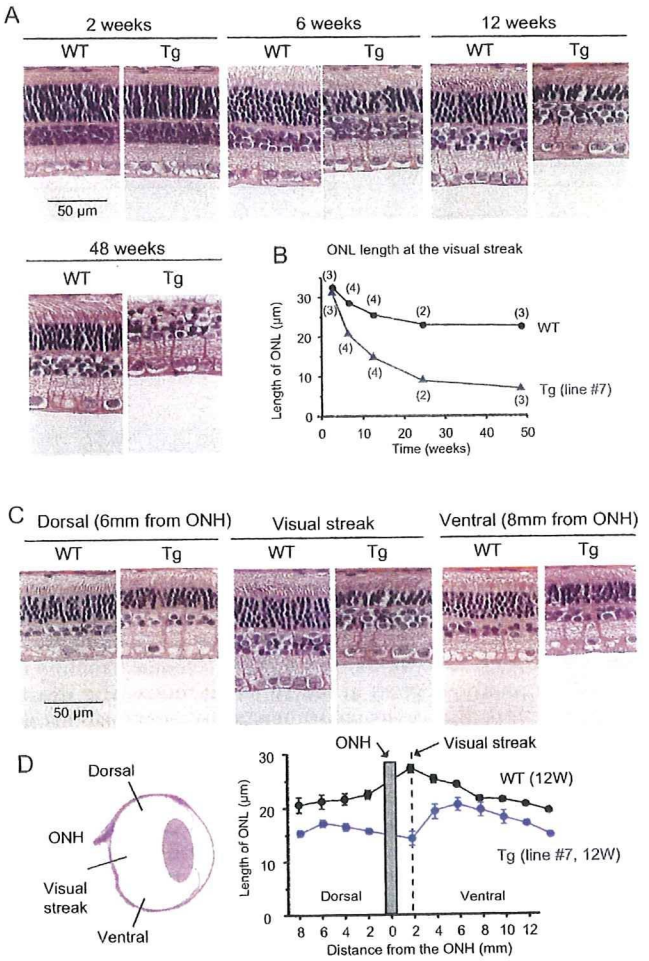

FIGURE 4. Retinal histology of Tg rabbits (line 7). (**A**) Retinal sections of WT and Tg rabbits at 2, 6, 12, and 48 weeks of age. (**B**) Changes in the thickness of the ONL at different ages (in weeks) for WT and Tg rabbits. The number of animals examined is shown in parentheses. (**C**) Vertical retinal sections 6 mm superior to the optic nerve head (ONH), at the visual streak, and 8 mm inferior to the ONH of 12-week-old WT and Tg rabbits. (**D**) Thickness of the ONL along the vertical meridian measured at 10 retinal locations at 2-mm intervals. Mean ± SEM of five WT and five Tg rabbits are plotted.

cone photoreceptors of Tg rabbits (Table 3). These results indicated a rod-dominant, progressive photoreceptor dysfunction in the retina of this line of Tg rabbits.

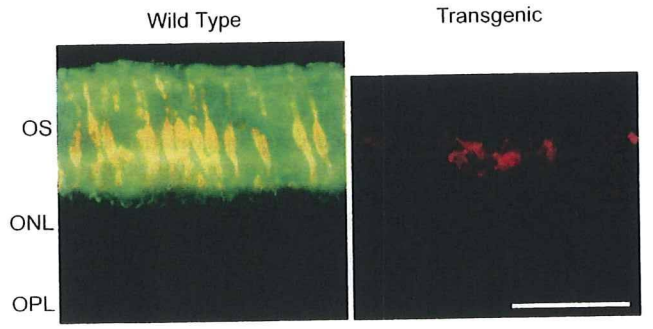

FIGURE 5. Immunohistochemical analysis of rod and cone photoreceptors double labeled with rhodopsin (*green*) and PNA (*red*) at the visual streak of 48-week-old WT (*left*) and transgenic (*right*) rabbits. Bar, 50 μm.

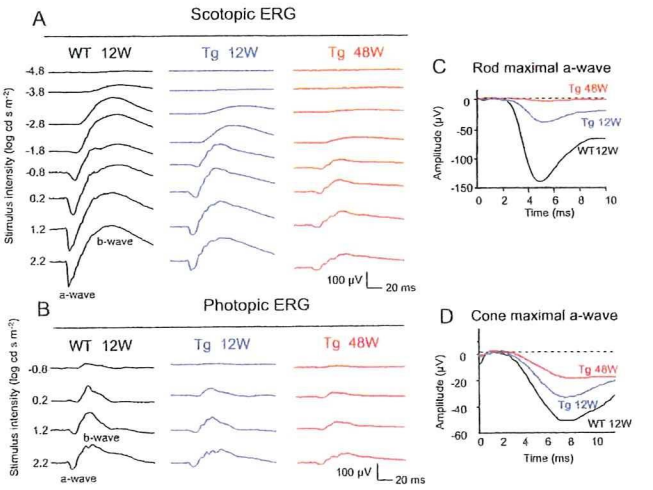

FIGURE 6. ERGs recorded from 12-week-old WT and 12- and 48-week-old rhodopsin P347L (line 7) Tg rabbits. (**A**) Scotopic ERGs elicited by eight different stimulus intensities. (**B**) Photopic ERGs elicited by four different stimulus intensities. (**C**) Rod maximum a-waves elicited by 2.2 log cd · s · m^{-2}. These responses were obtained by waveform subtraction of photopic ERGs from scotopic ERGs. (**D**) Cone maximum a-waves elicited by 2.2 log cd · s · m^{-2} on a rod-suppressing white background of 1.3 log cd · s · m^{-2}.

Presence of Extracellular Vesicles in the Tg Rabbit Retina

Finally, we compared the retinal ultrastructure of 6-week-old WT and line 7 Tg rabbits. The outer segments of the photoreceptors were slightly shorter and less organized in the retinas of 6-week-old Tg rabbits, although the outer segments still contained many well-packed discs at this age (Fig. 7A).

A striking finding in the Tg rabbit retina was the large number of small vesicles that accumulated in the extracellular space of the photoreceptors (Fig. 7A, asterisks). The vesicles were 50 to 300 nm in size and bound to a single membrane. We also found that these vesicles were cleaved from the membranes of the inner segments of the photoreceptors (Fig. 7B, arrows).

DISCUSSION

The purpose of this study was to generate a rabbit model of progressive retinal degeneration and to characterize the pattern of degeneration by using histology and electrophysiology. For this purpose, we used rabbit BAC transgenesis, which permitted us to produce a point mutation with no effect on the rest of the large rhodopsin gene, including the regulatory regions of the rhodopsin gene.[22–24] BAC transgenesis is known to provide high tissue- and stage-specific transgene expression that is independent of the site of integration and dependent on the number of integrated copies.[25]

We succeeded in generating six lines of Tg rabbits with different expression levels. Two lines showed high transgene expression levels and progressive retinal degeneration. Retinal histologic and ERG studies showed early loss of rod function associated with relatively preserved cone function, which is very similar to the clinical findings of human RP patients with the rhodopsin P347L mutation.[30,31] To the best of our knowledge, this is the first rabbit model of progressive retinal degeneration. Because rabbits have large eyes and are easy to handle and breed, we believe that our Tg rabbits are useful animal models for testing various new treatments, including surgical procedures.

TABLE 3. Summary of Photoreceptor Function Parameters in Tg Rabbits

	12 Wk		48 Wk	
	WT	Tg	WT	Tg
Rod log *Rm* (maximum response)	2.23 ± 0.08	1.63 ± 0.06*	2.06 ± 0.10	—†
Rod log *S* (sensitivity)	3.50 ± 0.04	3.19 ± 0.11*	3.42 ± 0.06	—†
Cone log *Rm* (maximum response)	1.73 ± 0.09	1.47 ± 0.07*	1.64 ± 0.08	1.21 ± 0.23*
Cone log *S* (sensitivity)	2.97 ± 0.05	2.84 ± 0.14	2.93 ± 0.10	2.68 ± 0.18*

Data are expressed as the mean ± SD. $n = 5$ for all.
* $P < 0.05$ (unpaired *t*-test).
† Rod photoreceptor responses in 48-week-old Tg rabbits were too small for the fitting model to be applied.

The fundus appearance and fluorescein angiograms were nearly normal in our Tg rabbits. The blood vessel diameters and optic disc appearance were examined monthly, and they were indistinguishable between WT and Tg rabbits at ages up to 40 weeks. An early sign of RP in human patients is an attenuation of blood vessel diameters in the eye. The normal diameter of the retinal vessels in our Tg rabbits may be due to the characteristics of rabbit retina, because retinal vessels in rabbits are confined to the horizontal myelinated bands, comprising optic axons, oligodendrocytes, and astrocytes, and are not associated with the inner retinal layers, as in vascular retinas.

In this study, we generated the transgenic rabbits on an albino background (NZW), because the rabbit BAC library was available only for NZW rabbits. However, this albino background may limit the model's usefulness. First, normal fundus coloring without any pigmentation in our Tg rabbits may have occurred because we used the nonpigmented NZW rabbits. Second, it is known that there are other anomalies in the visual system of albino rabbits, including lower ganglion cell densities[32] and aberrant optic decussation and retinal projections. To overcome these limitations, we are currently producing a pigmented line of Tg rabbits by mating our NZW Tg rabbits with pigmented Dutch rabbits.

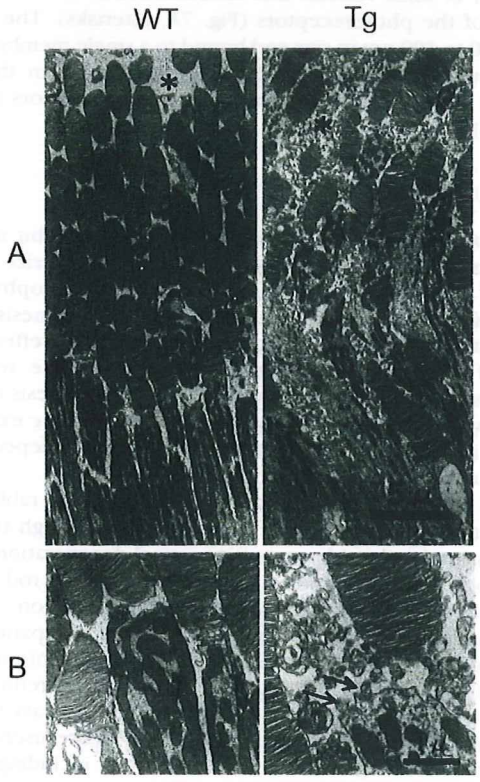

FIGURE 7. Ultrastructural analyses of 6-week-old WT (*left*) and Tg (*right*) rabbit retinas. (**A**) Tg rabbit retina showing many small vesicles accumulated in the extracellular space (*). (**B**) These abnormal vesicles were cleaved from the inner segment of photoreceptors (*arrows*).

By measuring the ONL thickness at different locations along the vertical meridian, we found a marked regional variation in the loss of photoreceptors in the Tg rabbit retina. The loss of photoreceptors was at its maximum near the visual streak, where the photoreceptor density is highest in WT rabbits. In contrast, the ONL thickness in Tg rabbits was relatively preserved in the peripheral retina (Figs. 4C, 4D). Similar regional variations in photoreceptor loss have been reported in other large animal models, including pigs and dogs.[16,17] Such regional variation in photoreceptor loss may be due to topographic variations in opsin expression, as reported by Timmers et al.,[33] and van Ginkel et al.,[34] who showed a central-to-peripheral gradient of rhodopsin mRNA levels in bovine retinas.

A distinct ultrastructural observation in the retina of Tg rabbits was the accumulation of numerous extracellular vesicles that were cleaved from the inner segments of the photoreceptors. At this stage, the outer segments still contained well-packed discs. These findings are consistent with findings in Tg mice with the P347S rhodopsin mutation.[35] Using two monoclonal antibodies against rhodopsin, Li et al.[35] demonstrated that these small vesicles contain rhodopsin, and they proposed that they were produced as a consequence of a defect in the transport of rhodopsin from the inner segment to the disc membranes of the outer segments. Although we have not yet examined whether the vesicles contain rhodopsin in our Tg rabbits, the similarity in the ultrastructural findings and site of rhodopsin mutation suggested that the defective delivery of opsin to the outer segment may be one of the causes of photoreceptor cell death in our Tg rabbits. However, other factors, including an overexpression of rhodopsin,[36,37] prolonged activation of phototransduction,[38] or activation of mislocalized opsin,[39] may be involved.

In conclusion, we have succeeded in generating a Tg rabbit model of retinal degeneration. Although further studies are needed to determine the exact mechanism of photoreceptor death observed in our model, we believe that our Tg rabbits will serve as a useful midsized animal model with which to study the pathophysiology of RP and develop novel treatments.

Acknowledgments

The authors thank Kensaku Kitada (Kitayama Labes Co., Ina, Japan) for breeding the Tg rabbits; Akira Shiota (PhoenixBio Co., Ltd. Utsunomiya, Japan) for technical help with BAC transgenesis; Robert E. Marc and Bryan W. Jones of Utah University for critical comments on the manuscript; and Duco I. Hamasaki of Miami University and Yozo Miyake of Shukutoku University for discussions of the manuscript.

References

1. Heckenlively JR. RP syndromes. In: Heckenlively JR, ed. *Retinitis Pigmentosa.* Philadelphia: JB Lippincott; 1988:221-252.
2. Weleber RG, Gregory-Evance K. Retinitis pigmentosa and allied disorders. In: Hinton DR, ed. *Basic Science and Inherited Retinal Disease: Retina.* Vol. 1, 4th ed. St. Louis: Mosby; 2006:395-498.
3. Hartong DT, Berson EL, Dryja TP. Retinitis pigmentosa. *Lancet.* 2006;368:1795-1809.
4. Daiger SP, Bowne SJ, Sullivan LS. Perspective on genes and mutations causing retinitis pigmentosa. *Arch Ophthalmol.* 2007;125:151-158.
5. Gal A, Apfelstedt-Sylla E, Janecke AR, Zrenner E. Rhodopsin mutations in inherited retinal dystrophies and dysfunctions. *Prog Retin Eye Res.* 1997;16:51-79.
6. Dryja TP, Hahn LB, Cowley GS, et al. Mutation spectrum of the rhodopsin gene among patients with autosomal dominant retinitis pigmentosa. *Proc Natl Acad Sci USA.* 1991;88:9370-9374.
7. Petersen-Jones SM. Animal models of human retinal dystrophies. *Eye.* 1998;12:566-570.
8. Chader GJ. Animal models in research on retinal degenerations: past progress and future hope. *Vision Res.* 2002;42:393-399.
9. Tao W, Wen R, Goddard MB, et al. Encapsulated cell-based delivery of CNTF reduces photoreceptor degeneration in animal models of retinitis pigmentosa. *Invest Ophthalmol Vis Sci.* 2002;43:3292-3298.
10. Bush RA, Lei B, Tao W, et al. Encapsulated cell-based intraocular delivery of ciliary neurotrophic factor in normal rabbit: dose-dependent effects on ERG and retinal histology. *Invest Ophthalmol Vis Sci.* 2004;45:2420-2430.
11. Acland GM, Aguirre GD, Ray J, et al. Gene therapy restores vision in a canine model of childhood blindness. *Nat Genet.* 2001;28:92-95.
12. Güven D, Weiland JD, Fujii G, et al. Long-term stimulation by active epiretinal implants in normal and RCD1 dogs. *J Neural Eng.* 2005;2:S65-73.
13. Narfström K. Hereditary progressive retinal atrophy in the Abyssinian cat. *J Hered.* 1983;74:273-276.
14. Menotti-Raymond M, David VA, Schäffer AA, et al. Mutation in CEP290 discovered for cat model of human retinal degeneration. *J Hered.* 2007;98:211-220.
15. Acland GM, Fletcher RT, Gentleman S, et al. Non-allelism of three genes (rcd1, rcd2 and erd) for early-onset hereditary retinal degeneration. *Exp Eye Res.* 1989;49:983-998.
16. Kijas JW, Cideciyan AV, Aleman TS, et al. Naturally occurring rhodopsin mutation in the dog causes retinal dysfunction and degeneration mimicking human dominant retinitis pigmentosa. *Proc Natl Acad Sci USA.* 2002;99:6328-6333.
17. Petters RM, Alexander CA, Wells KD, et al. Genetically engineered large animal model for studying cone photoreceptor survival and degeneration in retinitis pigmentosa. *Nat Biotechnol.* 1997;15:965-970.
18. Marc RE. Neurochemical stratification in the inner plexiform layer of the vertebrate retina. *Vision Res.* 1986;26:223-238.
19. Vaney DI, Young HM, Gynther IC. The rod circuit in the rabbit retina. *Vis Neurosci.* 1991;7:141-154.
20. Famiglietti EV, Sharpe SJ. Regional topography of rod and immunocytochemically characterized "blue" and "green" cone photoreceptors in rabbit retina. *Vis Neurosci.* 1995;12:1151-1175.
21. Rockhill RL, Daly FJ, MacNeil MA, et al. The diversity of ganglion cells in a mammalian retina. *J Neurosci.* 2002;22:3831-3843.
22. Yang XW, Model P, Heintz N. Homologous recombination based modification in Escherichia coli and germline transmission in transgenic mice of a bacterial artificial chromosome. *Nat Biotechnol.* 1997;15:859-865.
23. Zhang Y, Buchholz F, Muyrers JP, Stewart AF. A new logic for DNA engineering using recombination in Escherichia coli. *Nat Genet.* 1998;20:123-128.
24. Muyrers JP, Zhang Y, Benes V, et al. Point mutation of bacterial artificial chromosomes by ET recombination. *EMBO Rep.* 2000;1:239-243.
25. Giraldo P, Montoliu L. Size matters: use of YACs, BACs and PACs in transgenic animals. *Transgenic Res.* 2001;10:83-103.
26. Abe K, Hazama M, Katoh H, et al. Establishment of an efficient BAC transgenesis protocol and its application to functional characterization of the mouse Brachyury locus. *Exp Anim.* 2004;53:311-320.
27. Committee for Standardized Karyotype of Oryctolagus Cuniculus. Standard karyotype of the laboratory rabbit, Oryctolagus cuniculus. *Cytogenet Cell Genet.* 1981;31:240-248.
28. Hood DC, Birch DG. Rod phototransduction in retinitis pigmentosa: estimation and interpretation of parameters derived from the rod a-wave. *Invest Ophthalmol Vis Sci.* 1994;35:2948-2961.
29. Blanks JC, Johnson LV. Specific binding of peanut lectin to a class of retinal photoreceptor cells: a species comparison. *Invest Ophthalmol Vis Sci.* 1984:25;546-557.
30. Oh KT, Longmuir R, Oh DM, Stone EM, et al. Comparison of the clinical expression of retinitis pigmentosa associated with rhodopsin mutations at codon 347 and codon 23. *Am J Ophthalmol.* 2003;136:306-313.
31. Berson EL, Rosner B, Sandberg MA, et al. Ocular findings in patients with autosomal dominant retinitis pigmentosa and rhodopsin, proline-347-leucine. *Am J Ophthalmol.* 1991;111:614-623.
32. Oyster CW, Takahashi ES, Fry KR, Lam DM. Ganglion cell density in albino and pigmented rabbit retinas labeled with a ganglion cell-specific monoclonal antibody. *Brain Res.* 1987:425;25-33.
33. Timmers AM, Wintjes ET, Hauswirth WW. Fetal topography of bovine rhodopsin mRNA suggests retinotopographically determined gene expression. *Invest Ophthalmol Vis Sci.* 1995;36:2008-2019.
34. van Ginkel PR, Timmers AM, Szél A, Hauswirth WW. Topographical regulation of cone and rod opsin genes: parallel, position dependent levels of transcription. *Brain Res Dev Brain Res.* 1995;89:146-149.
35. Li T, Snyder WK, Olsson JE, Dryja TP. Transgenic mice carrying the dominant rhodopsin mutation P347S: evidence for defective vectorial transport of rhodopsin to the outer segments. *Proc Natl Acad Sci USA.* 1996;93:14176-14181.
36. Olsson JE, Gordon JW, Pawlyk BS, et al. Transgenic mice with a rhodopsin mutation (Pro23His): a mouse model of autosomal dominant retinitis pigmentosa. *Neuron.* 1992;9:815-830.
37. Tan E, Wang Q, Quiambao AB, et al. The relationship between opsin overexpression and photoreceptor degeneration. *Invest Ophthalmol Vis Sci.* 2001;42:589-600.
38. Chen J, Makino CL, Peachey NS, Baylor DA, Simon MI. Mechanisms of rhodopsin inactivation in vivo as revealed by a COOH-terminal truncation mutant. *Science.* 1995;267:374-377.
39. Alfinito PD, Townes-Anderson E. Activation of mislocalized opsin kills rod cells: a novel mechanism for rod cell death in retinal disease. *Proc Natl Acad Sci USA.* 2002;99:5655-5660.

Supernormal ERG Oscillatory Potentials in Transgenic Rabbit with Rhodopsin P347L Mutation and Retinal Degeneration

Takao Sakai, Mineo Kondo, Shinji Ueno, Toshiyuki Koyasu, Keiichi Komeima, and Hiroko Terasaki

Purpose. To determine the properties of the retina of a rhodopsin P347L transgenic (Tg) rabbit model of retinal degeneration by electroretinography (ERG).

Methods. Full-field ERGs were recorded in 12- to 48-week-old wild-type (WT) and Tg rabbits. The a-wave was analyzed by the a-wave fitting model of Hood and Birch. The stimulus–response function of the b-wave was analyzed by the Michaelis-Menten equation. Oscillatory potentials (OPs) were extracted by digital filtering after subtracting the a-wave. OPs were also recorded before and after an intravitreal injection of L-2 amino-4-phosphonobutyric acid (APB), *cis*-2,3 piperidine dicarboxylic acid (PDA), γ-amino butyric acid (GABA), or tetrodotoxin citrate (TTX).

Results. All the ERG components of Tg rabbits decreased progressively with age with the a-wave more affected than the b-wave, and the OPs were most preserved. Of interest, the summed OP amplitudes of the Tg rabbits were significantly larger than those of WT rabbits when they were 12 weeks of age. The changes in the amplitudes of the OPs after intravitreal injections of APB, PDA, or GABA in Tg rabbits did not differ significantly from those of WT rabbits. However, injection of TTX resulted in a significantly larger amplitude reduction of the OPs in Tg (65.3%) than in WT (28.6%) rabbits.

Conclusions. The significantly larger OPs in Tg rabbits resulted from alterations in the inner retinal neurons. The greater effect of TTX on the OP amplitudes in Tg rabbits suggests that the supernormal OPs in Tg rabbits may be related to secondary changes in the spiking neurons of the inner retina after photoreceptor degeneration. (*Invest Ophthalmol Vis Sci.* 2009;50: 4402–4409) DOI:10.1167/iovs.09-3458

Electrophysiological assessments of human patients and animal models of retinitis pigmentosa (RP) are valuable for understanding the pathophysiology of RP because layer-by-layer retinal function can be evaluated objectively. The photoreceptor components of the electroretinogram (ERG) are usually most severely impaired in patients with RP, even at the early stages,[1–4] because this disease primarily affects the photoreceptor–retinal pigment epithelium complex.[1–7] ERG studies have also shown that not only the photoreceptors, but also the bipolar cells can be affected in patients with RP.[8–11] However, there have been reports of an unexpected preservation or even an enhancement of the postreceptoral ERG components in some animal models of RP. These components include the b-wave,[12–14] the scotopic threshold response (STR),[15] the negative component of the photopic ERG,[16] and oscillatory potentials (OPs).[17] The exact mechanism(s) underlying these secondary functional changes in the postreceptoral neurons after the photoreceptor degeneration has not been fully determined.

We have recently succeeded in generating a rhodopsin P347L transgenic (Tg) rabbit by using bacterial artificial chromosome (BAC) transgenesis.[18] We have shown that the rod function of Tg rabbits was reduced at an early age, whereas the cone function was relatively well preserved. This sequence of alterations is similar to those in human patients with RP with the rhodopsin P347L mutation.[19,20] However, we did not analyze the properties of all the ERG components quantitatively and did not compare them with age-matched wild-type (WT) rabbits.

The purpose of this study was to investigate the properties of the ERGs of our Tg rabbits. We analyzed the a- and b-waves, and the OPs which originate from inner retinal neurons[21–25] until ~48 weeks of age. All ERG components of Tg rabbits progressively decreased with increasing age, and the a-wave was more severely impaired than the b-wave. Of note, the OP amplitudes of Tg rabbits were larger than those of WT rabbits when they were 12 weeks of age. The results of pharmacologic studies suggest that the functional changes in the TTX-sensitive spiking neurons of the inner retina contribute to the supernormal OPs in young Tg rabbits.

Materials and Methods

Animals

The experiments were performed on 31 Tg and 31 WT New Zealand White rabbits. The ages of the rabbits ranged from 12 to 48 weeks. Thirty animals were used for full-field ERG recordings without any treatment and 32 for pharmacologic studies. This study was conducted in accordance with the ARVO Statement on the Use of Animals in Ophthalmic and Vision Research. All protocols were approved by the Institutional Review Board of Nagoya University Graduate School of Medicine.

Our techniques for generating of Tg rabbits has been described in detail.[18] Briefly, a rabbit BAC clone that included the entire rhodopsin gene was identified, and a C-to-T transition at the codon of proline 347 was performed by BAC recombineering.[26–28] This transition in exon 5 of the rabbit rhodopsin gene resulted in a proline-to-leucine substitution at codon 347. After the BAC modification in *Escherichia coli*, the linearized BAC Tg construct was purified and injected into rabbit embryos at the pronucleus stage.

Southern blot analysis showed that 12 of 80 newborn rabbits were transgene positive, and 10 of the 12 survived. These 10 founders were

From the Department of Ophthalmology, Nagoya University Graduate School of Medicine, Nagoya, Japan.

Supported by Health Sciences Research Grants 18591913 and 18390466 (H16-sensory-001) from the Ministry of Health, Labor and Welfare and the Ministry of Education, Culture, Science and Technology, Japan.

Submitted for publication January 26, 2009; revised March 28, 2009; accepted July 9, 2009.

Disclosure: **T. Sakai**, None; **M. Kondo**, None; **S. Ueno**, None; **T. Koyasu**, None; **K. Komeima**, None; **H. Terasaki**, None

The publication costs of this article were defrayed in part by page charge payment. This article must therefore be marked "*advertisement*" in accordance with 18 U.S.C. §1734 solely to indicate this fact.

Corresponding author: Mineo Kondo, Department of Ophthalmology, Nagoya University Graduate School of Medicine, 65 Tsuruma-cho, Showa-ku, Nagoya 466-8550, Japan; kondomi@med.nagoya-u.ac.jp.

Investigative Ophthalmology & Visual Science, September 2009, Vol. 50, No. 9

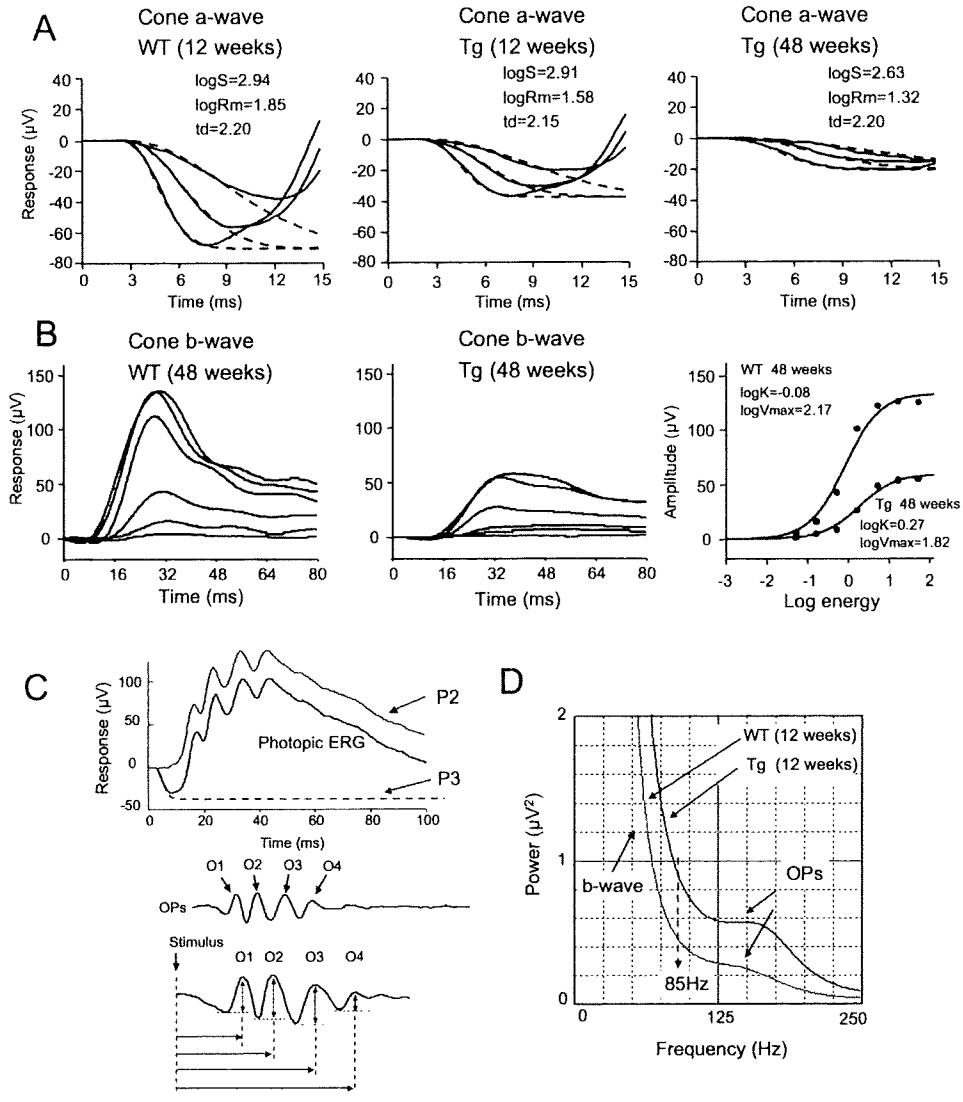

FIGURE 1. Analyses of ERG components. (**A**) Cone ERG a-waves (*solid lines*) recorded from 12-week-old WT, 12-week-old Tg, and 48-week-old Tg rabbits. Responses to three brighter stimuli of 2.2, 1.7, and 1.2 log cd s m^{-2} are shown. *Dashed lines*: best fit of equation 1 to the entire data set. The coefficients for the best fit are shown in each panel. (**B**) Cone ERG b-waves recorded from a 48-week-old WT (*left*) and Tg (*middle*) rabbits. Responses to seven flashes of −1.3 to 1.7 log cd s m^{-2} are shown. *Right*: best fit of equation 2 to the amplitude of the b-waves. (**C**) Extraction and analysis of the OPs of the photopic ERG. To minimize the effect of a-wave contamination, the photoreceptor component (equation 1, P3) was digitally subtracted from the intact ERG (*top*). The amplitude of the individual OP was defined as the difference between the peak and the trough immediately preceding it (*bottom*). (**D**) Frequency spectra of the photopic ERG P2 component in WT and Tg rabbits. The OPs were extracted by band-pass filtering of 85 to 300 Hz.

bred with WT rabbits, and six founders were shown to have transmitted the transgene. We mainly reproduced and investigated line 7, which had the highest level of transgene expression and the most severe photoreceptor degeneration as determined histologically.[18]

ERG Recordings

Animals were dark adapted for 60 minutes and then anesthetized with an intramuscular injection of 25 mg/kg ketamine and 2 mg/kg xylazine. ERGs were recorded with Burian-Allen bipolar contact lens electrodes (Hansen Laboratory, Iowa, City, IA). The animals were placed in a Ganzfeld bowl and stimulated with stroboscopic stimuli (model SG-2002; LKC Technologies, Gaithersburg, MD). The stimulus strength at the cornea was 2.2 log cd s m^{-2} (photopic units). Sixteen steps (0.5 log unit steps) of stimuli ranging from −5.3 to 2.2 log cd s m^{-2} were used to elicit the scotopic ERGs. The photopic ERGs were then recorded on a rod-suppressing white background of 3.3 log scot td, and seven steps of stimuli ranging from −0.8 to 2.2 log cd s m^{-2} were used. Signals were amplified, band-pass filtered between 0.3 to 1000 Hz, and averaged by using a computer-assisted signal analysis system (MEB-9100, Neuropack; Nihon Kohden, Tokyo, Japan).

Fitting Model to a- and b-Waves

To evaluate photoreceptor function, the leading edge of the rod and cone a-waves was fitted to a curve by the Hood and Birch modification[2] of the Lamb and Pugh model (Fig. 1A)[29]:

$$P3(i, t) = \{1 - \exp[-i \cdot S(t - t_d)^2]\}Rm \quad \text{for} \quad t > t_d \qquad (1)$$

In this equation, i is the flash energy (log phot cd s m^{-2}); t_d is the time delay; t is the time after the flash onset; S is the sensitivity; and Rm is the maximum response amplitude. This model yields values for Rm, S, and t_d. For more details, see the Appendix.

The stimulus-response function of the rod and cone b-waves was fitted by the Michaelis-Menten equation (Fig. 1B)[30,31]:

$$V = V_{max} \cdot I/(I + K) \qquad (2)$$

where V is the amplitude of the b-wave; V_{max} is the maximum amplitude of the b-wave; I is the flash energy (log phot cd s m^{-2}); and K is the flash energy that elicits a b-wave amplitude of half V_{max} (half-saturation coefficient). This model yielded values for two parameters: V_{max} and K. For responses to higher flash energies at which substantial a-wave intrusion occurred, the photorecepter component (P3) was digitally subtracted. High-frequency OPs (85–300 Hz) were also removed by digital filtering.

Extraction and Measurement of Photopic OPs

The OPs were extracted by using the method of Zhang et al.[23] and Akula et al.[32] To reduce the contamination of the a-wave on the early OPs, we fitted a mathematical model of the a-wave (equation 1) and

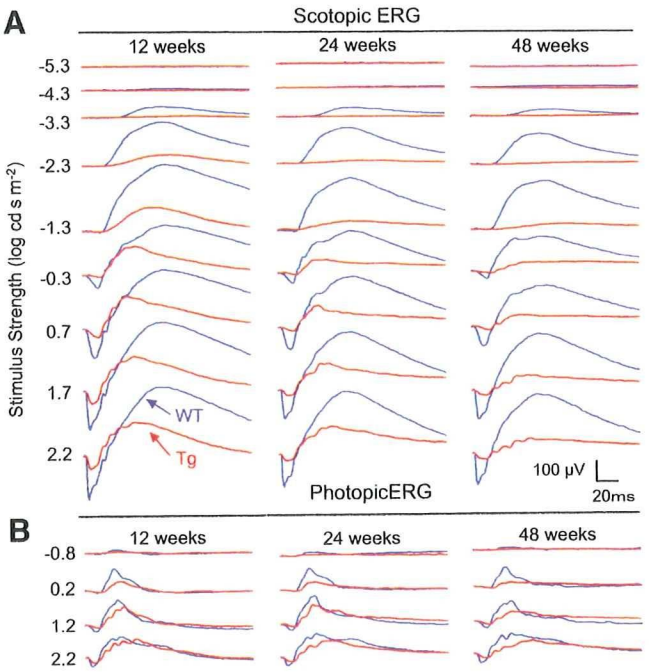

FIGURE 2. ERGs recorded from 12-, 24-, and 48-week-old WT (*blue*), and rhodopsin P347L transgenic (Tg, *red*) rabbits. (**A**) Scotopic ERGs elicited by nine different stimulus strengths. (**B**) Photopic ERGs elicited by four different stimulus strengths.

digitally subtracted the a-wave component from the intact ERG (Fig. 1C, top).

To determine appropriate band-pass filters for extracting OPs of WT and Tg rabbits, we analyzed the extracted postreceptoral component (P2) by Fast Fourier Transform (FFT). We found that the OPs of the photopic ERG of WT and Tg rabbits have one main peak (Fig. 1D). Based on these results, we chose band-pass settings of 85 to 300 Hz for extracting the photopic OPs which are similar to those used in a recent rabbit ERG study.[22,23]

To measure each OP amplitude (O1-O4), we measured the amplitude of a specific OP from the peak and trough immediately preceding it (Fig. 1C, bottom). The implicit time was defined as the time from stimulus onset to the peak of the OP. The summed OP amplitude was also used to assess total OP function.

Drug Applications

The drugs and intravitreal injection techniques have been described in detail.[22,24,33-35] The drugs were injected into the vitreous with a 30-gauge needle inserted through the pars plana ~1 mm posterior to the limbus. The drugs (Sigma-Aldrich, St. Louis, MO; Sankyo Co., Ltd., Tokyo, Japan) were dissolved in sterile PBS and injected in 0.05 mL. The intravitreal concentrations were: 2 mM for L-2 amino-4-phosphonobutyric acid (APB); 4 mM for *cis*-2,3 piperidine dicarboxylic acid (PDA); 2 mM for γ-amino butyric acid (GABA); and 2 μM for tetrodotoxin citrate (TTX).

Recordings were begun approximately 60 to 90 minutes after the drug injections, and the studies were completed within 3 hours. We used rabbit eyes that had not been previously treated.

Statistical Analyses

Unpaired Student's *t*-test with Bonferroni's correction was used to compare the amplitudes or implicit times of each ERG component between WT and Tg rabbits. Differences were considered to be significant when $P < 0.05$.

RESULTS

Scotopic and Photopic ERGs

Scotopic and photopic ERGs elicited by different stimulus strengths from 12-, 24-, and 48-week-old WT (blue) and Tg (red) rabbits are shown in Figure 2. The amplitudes of both the scotopic and photopic ERGs of the Tg rabbits were smaller than those of the WT rabbits. In addition, there was a progressive decrease in the amplitudes with increasing age. The scotopic ERGs were more severely affected than the photopic ERGs in Tg. At 48 weeks, the scotopic b-waves at lower stimulus strengths (-5.3 to -1.3 log cd s m^{-2}) were nearly nondetectable, and at the maximum stimulus strength, the scotopic ERG was almost the same as the photopic ERG in Tg rabbits. This indicated that the rod function was nearly extinguished at 48 weeks in Tg rabbits, and the cones were relatively well preserved.

Analyses of a- and b-Waves

The a-wave that was fitted to a curve by the Hood and Birch[2] method showed that the rod maximum amplitude (*Rm*) of Tg rabbits was already reduced by 0.60 log units (% reduction, 75%) at 12 weeks, and by 1.01 log units (90%) at 24 weeks (Fig. 3A, Table 1). At 48 weeks, the maximum amplitude of rod a-wave of all Tg rabbits was <10 μV, which was too small to apply the fitting model. In contrast, the cone *Rm* of Tg rabbits was reduced by only 0.26 log unit (45%) at 12 weeks and by 0.43 log unit (63%), even at 48 weeks of age (Fig. 3A, Table 1; see also the Appendix). We also found that not only the *Rm*, but also the transduction sensitivity (*S*) were abnormal in both rod and cone photoreceptors of Tg rabbits, especially at 24 weeks and older (Table 1).

The b-wave analysis using the Michaelis-Menten equation[30,31] showed that both the maximum amplitude (V_{max}) and half-saturation coefficient (*K*) of the rod b-wave was significantly abnormal in Tg rabbits at 24 weeks and later, and the difference between two types of rabbits increased with increasing age (Fig. 3B, Table 1). In contrast, there was no significant difference in the cone b-wave V_{max} between Tg and

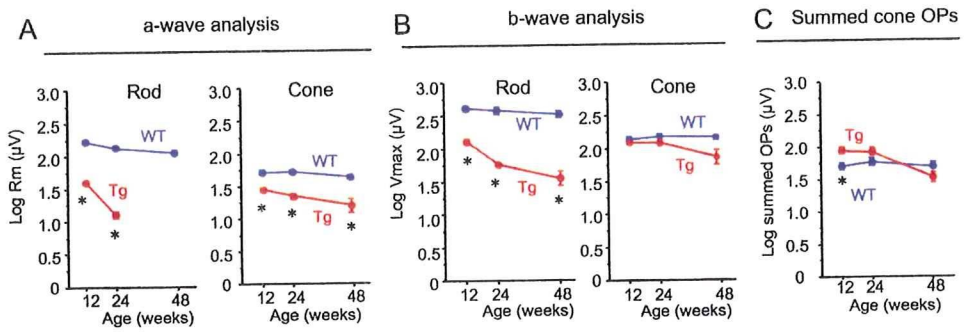

FIGURE 3. Plots of maximum amplitude of each ERG components. Mean values of five animals are plotted. Bars, SEM. *$P < 0.05$ (unpaired *t*-test with Bonferroni's correction). (**A**) Plots of log maximum amplitude for rod and cone a-waves (*Rm*) for rabbits at 12, 24, and 48 weeks of age. (**B**) Plots of log maximum amplitude for rod and cone b-waves (V_{max}) for rabbits at 12, 24, and 48 weeks of age. (**C**) Plots of log summed OPs of cone ERG at 12, 24, and 48 weeks of age.

TABLE 1. Summary of ERG Parameters in WT and Tg Rabbits

	12 Weeks		24 Weeks		48 Weeks	
	WT (n = 5)	Tg (n = 5)	WT (n = 5)	Tg (n = 5)	WT (n = 5)	Tg (n = 5)
a-Wave analysis						
Rod log Rm	2.23 ± 0.08	1.63 ± 0.06*	2.14 ± 0.07	1.13 ± 0.12*	2.06 ± 0.10	—†
Rod log S	3.50 ± 0.04	3.19 ± 0.11*	3.46 ± 0.15	3.29 ± 0.09*	3.42 ± 0.06	—†
Cone log Rm	1.73 ± 0.09	1.47 ± 0.07*	1.75 ± 0.07	1.36 ± 0.10*	1.64 ± 0.08	1.21 ± 0.23*
Cone log S	2.97 ± 0.05	2.84 ± 0.14	2.91 ± 0.09	2.75 ± 0.07*	2.93 ± 0.10	2.68 ± 0.18*
b-Wave analysis						
Rod log V_{max}	2.61 ± 0.07	2.11 ± 0.09*	2.58 ± 0.12	1.76 ± 0.06*	2.51 ± 0.12	1.62 ± 0.22*
Rod log K	−2.43 ± 0.15	−1.96 ± 0.42	−2.20 ± 0.21	−1.87 ± 0.13*	−2.21 ± 0.20	−1.80 ± 0.18*
Cone log V_{max}	2.16 ± 0.10	2.12 ± 0.04	2.22 ± 0.06	2.12 ± 0.08	2.18 ± 0.07	1.89 ± 0.23
Cone log K	−0.22 ± 0.10	0.16 ± 0.08*	−0.13 ± 0.14	0.32 ± 0.07*	−0.11 ± 0.08	0.33 ± 0.17*
Summed OPs						
Log Σ OPs	1.71 ± 1.35	1.96 ± 1.10*	1.78 ± 1.24	1.94 ± 1.43	1.71 ± 1.10	1.56 ± 1.40

Data are expressed as the mean ± 1 SD.

* $P < 0.05$, unpaired t-test with Bonferroni's correction.

† Rod photoreceptor responses in 48-week-old Tg rabbits were too small to apply the fitting model.

Wt rabbits at 12 to 48 weeks, although the K was already reduced significantly at 12 weeks (Fig. 3B, Table 1).

These results indicated that the function of both the rod and cone components of the Tg rabbits decreased with age, and the rod components was more severely affected than the cone components.

Supernormal OPs in Tg Rabbits

We next analyzed the OPs, which are believed to originate from inner retinal neurons including the amacrine and ganglion cells.[21–25]

The photopic ERGs elicited by the maximum stimulus strength of 2.2 log cd s m^{-2} from five WT and Tg rabbits at 12 weeks of age are shown in Figure 4A. The a-wave amplitudes of the cone ERGs of Tg rabbits were smaller than those of WT rabbits, whereas the b-wave amplitudes were nearly the same in the two types of rabbit (see also Figs. 2, 3). The OPs were more prominent in the Tg than in the WT rabbits. We then extracted the OPs by digital filtering after subtracting the a-wave (Figs. 1C, 1D), and confirmed that the summed OP amplitudes in Tg were noticeably larger than those in WT rabbits (Fig. 4B). The summed OP amplitude was 90.5 ± 22.5 μV (mean ± SD, n = 5) in Tg rabbits which was significantly larger than the 51.4 ± 13.0 μV in WT rabbits (P = 0.009). At 24 to 48 weeks, the summed OP amplitudes of Tg were not significantly different from those of WT rabbits (Fig. 3C, Table 1).

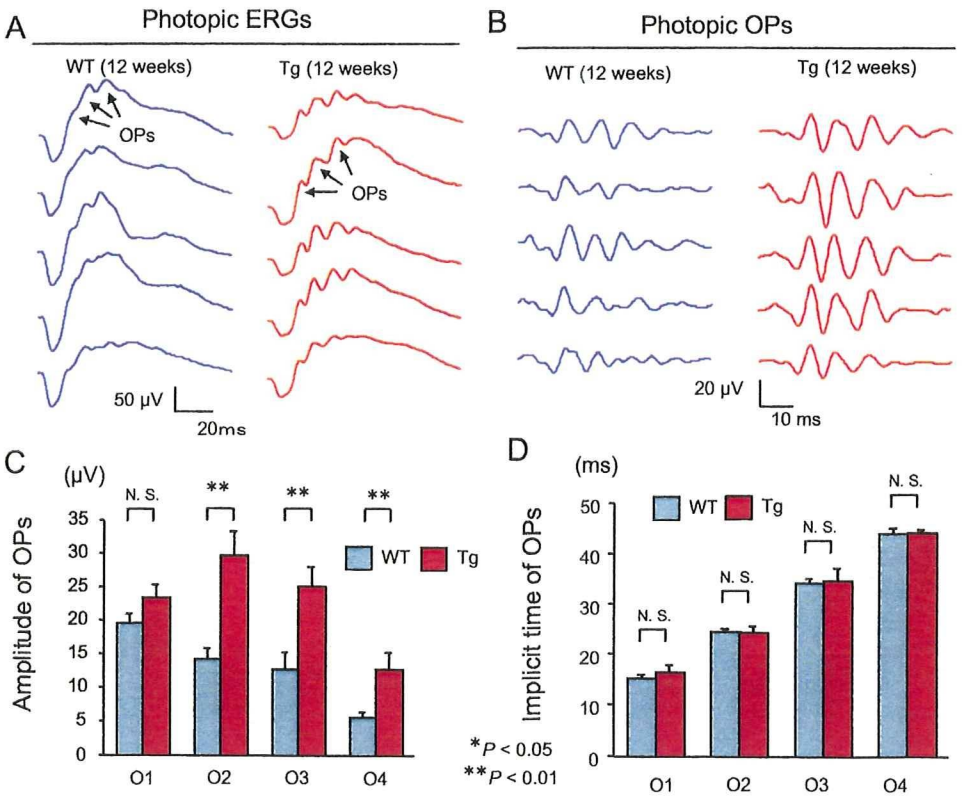

FIGURE 4. Supernormal OPs in Tg rabbits. (**A**) Photopic ERGs (**B**) extracted OPs, (**C**) mean amplitudes of individual OPs (O1–O4) and (**D**) mean implicit times of individual OPs (O1–O4) for five WT and Tg rabbits of 12 weeks of age. Bars, SEM.

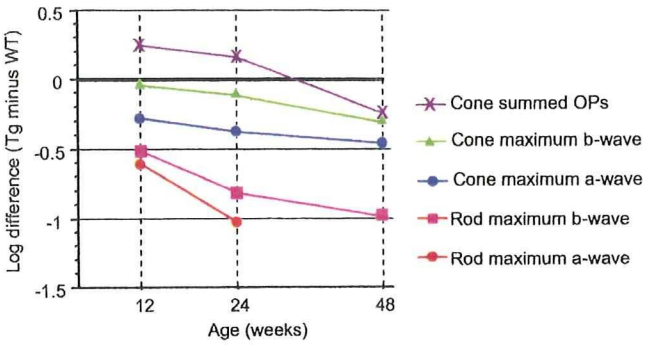

FIGURE 5. Difference of the log maximum amplitude between Tg and WT rabbits for all ERG components. Values of Tg minus WT are shown. The minus values indicate that the amplitudes of the WT rabbits were larger than those of Tg rabbits.

We also compared the amplitude of the individual Ops (O1-O4) between the WT and Tg rabbits, because there are reports suggesting that each OP wavelet may have different retinal origins.[21,22,36] We found that the amplitude for the later three OPs (O2-O4) in Tg rabbits were significantly larger than the corresponding OPs in the WT rabbits. However, the amplitude of O1 was not different between the two types of rabbits (Fig. 4C).

The implicit times of the OPs did not differ between the two types of rabbits for all the OPs (Fig. 4D).

We also compared the summed OP amplitudes of scotopic OPs between WT and Tg rabbits when they were 12 weeks old, but there was no statistically significant difference (WT, 86.2 ± 16.3 μV; Tg, 73.6 ± 18.9 μV, mean ± SD, $P = 0.25$).

Comparisons of Amplitudes of Each ERG Component

The differences in the log maximum amplitude between WT and Tg rabbits for all ERG components (rod a-wave, cone a-wave, rod b-wave, cone b-wave, and cone OPs) are shown in Figure 5. In these graphs, the values of Tg minus WT are plotted. A minus value means that the amplitude in WT is larger than that in Tg rabbits. As expected, the differences became smaller for all ERG components with increasing age, and the rod components were more severely affected than the cone components in Tg rabbits. We also found that and the a-waves were more affected than the b-waves, and OPs were better preserved than the a- and b-waves in Tg rabbits. Tg rabbits had supernormal OPs amplitude when they were 12 and 24 weeks of age.

Effect of Pharmacologic Agents on OPs of WT and Tg Rabbits

Finally, to determine what types of retinal cells or circuits are involved in the enhanced OP amplitudes in Tg rabbits, we studied the effect of various pharmacologic agents on the OPs of WT and Tg rabbits when they were 16 weeks of age. Before the drug injections, we confirmed that the intravitreal injection of PBS alone did not change the amplitude and waveform of photopic OPs for two rabbits (data not shown).

APB is a mGluR6 agonist that blocks synaptic transmission between photoreceptors and ON bipolar cells, leaving the OFF pathway intact.[37] Intravitreal injection of APB reduced all photopic OPs almost completely in both WT and Tg rabbits (Fig. 6A, 6B). These changes indicated that the postsynaptic ON-pathway plays an important role in the origin of the photopic OPs[22,24,38,39] in WT and Tg rabbits.

PDA is an antagonist of AMPA/KA class ionotropic glutamate receptors and blocks the light driven response of OFF-bipolar cells, horizontal cells, and many amacrine and ganglion cells. The ON bipolar cells were relatively unaffected.[33,40] An intravitreal injection of PDA also greatly reduced the amplitude of the photopic OPs,[22,24] but to a lesser extent than APB (Fig. 6A). The degree of amplitude reduction by PDA was not different in the WT and Tg (Fig. 6B) rabbits.

GABA is a neurotransmitter released from retinal amacrine cells and horizontal cells.[41] As reported in other studies,[21] GABA suppressed the OPs in both WT and Tg rabbits (Fig. 6A). Again, the degree of reduction of the OPs by GABA was not different between the WT and Tg rabbits (Figs. 6B).

TTX blocks voltage-gated sodium channels, and thus blocks action potentials produced by ganglion cells and certain classes of amacrine cells.[42-48] An intravitreal injection of TTX resulted in the reduction in the amplitude of the photopic OPs (Fig.

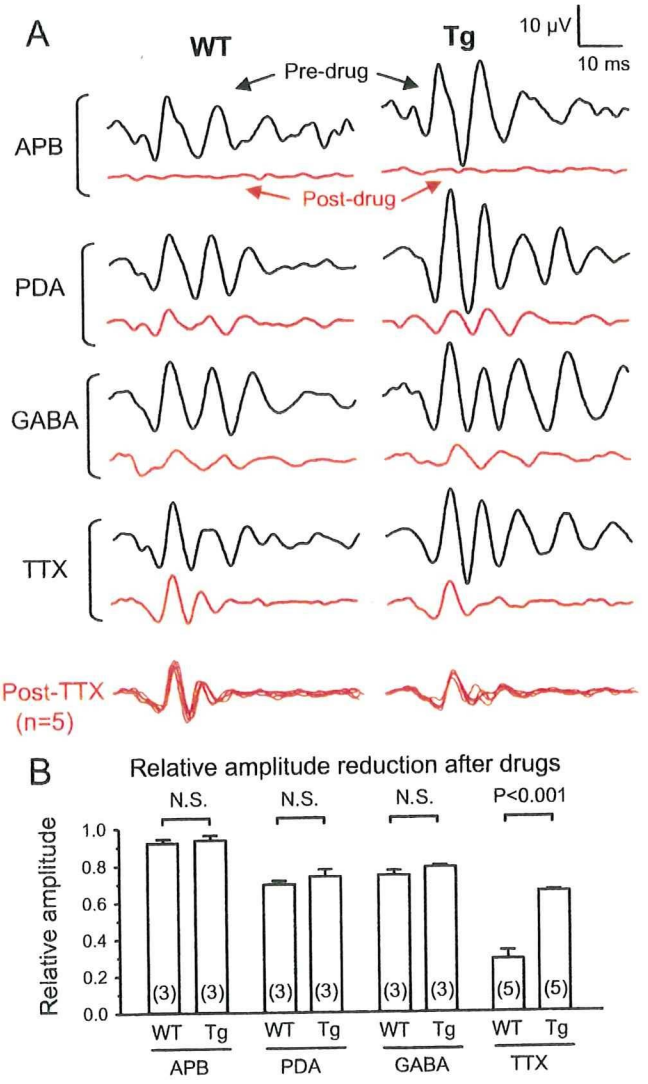

FIGURE 6. Effects of various pharmacologic agents on the cone OPs of WT and Tg rabbits. (**A**) Representative waveforms of OPs before (*black*) and after (*red*) APB, PDA, GABA, or TTX. The post-TTX recordings from five different rabbits are superimposed in the *bottom* panel. Note that the OP amplitudes of Tg rabbits are smaller than those of WT rabbits after TTX. (**B**) Plots of relative amplitude reduction after drugs in WT and Tg rabbits. Data are the mean ± SEM. The numbers in the parenthesis indicate the number of animals used. The effect of TTX on the amplitude reduction of OPs in Tg rabbits was significantly larger than in WT rabbits.

6A). As reported,[22] the effect of TTX was greater for the later OPs (O3 and O4) in both WT and Tg rabbits (Fig. 6A). We found that the degree of amplitude reduction by TTX was very different between the two types of rabbits: the amplitude reduction by TTX was only 28.6% ± 10.2% in WT, but was 65.3% ± 2.0% in Tg rabbits (mean ± SD, $n = 5$, Fig. 6B). This difference was statistically significant ($P < 0.001$). As a consequence, the summed OP amplitudes in Tg rabbit after TTX (25.5 ± 6.6 μV) became smaller than those of WT rabbits (37.7 ± 3.0 μV). The OP waveforms after TTX from the five animals are superimposed in the bottom panel of Figure 6A. These results suggested that the functional changes in the TTX-sensitive spiking neurons may be related to the enhanced photopic OPs in our young Tg rabbits.

Effect of TTX on the Photopic ERG b-Wave in WT and Tg Rabbits

It has been reported that TTX reduces the photopic ERG b-wave in rats,[46–48] indicating that voltage-gated sodium channels normally boost the photopic b-wave amplitude. We thought that if the amplitude reduction of the photopic ERG b-wave by TTX was larger in Tg than in WT rabbits, it could suggest that the supernormal OPs of Tg rabbits are caused by enhanced input from bipolar cells to the inner retina. We studied the effect of TTX on the amplitude of photopic ERG b-wave in our rabbits, and found that TTX reduced the amplitude of the photopic ERG b-wave for both WT and Tg rabbits. However, the degree of amplitude reduction by TTX was not different between WT (60.0% ± 7.3%, $n = 5$) and Tg (54.6% ± 13.9%, $n = 5$, $P = 0.55$) rabbits.

Discussion

Our results demonstrated that the a- and b-waves of the ERGs of Tg rabbits decrease progressively with increasing age, and the rod components were more affected than the cone components. These changes are characteristic of animal models of RP and human patients with RP.[1–4] In addition, the degree of amplitude reduction was greater for the a-wave (photoreceptor component) than for the b-wave (bipolar cell component). Such a difference in reduction in the amplitude of the a- and b-waves has been previously reported,[12–14] and may be explained by the difference in the stimulus-response function of the a- and b-waves. A past study using a computational model of the a- and b-waves indicated that there should be relatively little change in V_{max} with changes in Rm, because the photoreceptor response are linear over the range of the b-wave V-log I function.[49]

The most interesting finding in this study was the enhanced amplitudes of the OPs in young Tg rabbits. The amplitudes of summed OPs of 12-week-old Tg were 1.76 times (0.25 log unit) larger than those of WT rabbits of the same age. At this age, the maximum cone a-wave amplitude of Tg rabbits was significantly smaller than that of WT rabbits, and the maximum cone b-wave amplitude of Tg rabbits was about the same amplitude as that of WT rabbits. The supernormal amplitude of the OPs cannot be explained simply by the buffering effect of inner retinal neurons[12,13] and suggest that there are most likely secondary functional changes in the inner retinal neurons.

Banin et al.[17] have reported similar ERG findings in their pig RP model with a rhodopsin mutation. They observed supernormal photopic OPs and abnormal cone b-wave waveforms even at early stages of retinal degeneration when the photoreceptor physiology was still completely normal. They suggested that the rod photoreceptor degeneration may cause the functional changes in the inner retina of the cone circuitry even at early stages of retinal degeneration. Although they did not measure the amplitude of the OPs quantitatively, the pattern of the changes of the OPs in their pig model were very similar to those in our Tg rabbit: the early OP (O1) in the Tg did not differ significantly from that of WT, but the later OPs (O2–O4) were clearly larger in Tg (see Fig. 2e in Ref. 17 and our Fig. 4). It is very interesting that the same point mutation near the C-terminal of rhodopsin gene, P347L, can cause similar secondary functional changes in the inner retina in two different species of RP models: the pig and the rabbit.

To determine what types of retinal cells or circuits might contribute to the supernormal OPs in young Tg rabbits, we injected different various pharmacologic agents into the eye of WT and Tg rabbits. Our results in WT rabbits were consistent with the conclusions of earlier reports that the OPs originate mainly from third-order neurons of the inner retina, predominantly in the ON-pathway.[21–24,36] A direct contribution from cone ON- and OFF-bipolar cells to the rabbit cone OPs must not be large, because APB or PDA alone resulted in a severe amplitude reduction of the OPs. We also found that whereas the degree of the ERG reduction after APB, PDA, and GABA did not differ between Tg and WT rabbits, TTX application resulted in dramatic differences in the degrees of amplitude change in the two types of rabbits. The degree of amplitude reduction was significantly greater in Tg (65.3%) than in WT (28.6%) rabbits. As a result, the summed amplitude of the OPs in Tg became significantly smaller than that of WT after TTX. These results suggest that the functional changes in the TTX-sensitive retinal neurons, may contribute to the abnormally large OPs in young Tg rabbits.

A possible mechanism for supernormal OPs in our Tg rabbits is the changes in the input from ON/OFF bipolar cells to the OP generator in the inner retina. First, we compared the activity of cone ON bipolar cells (cone V_{max}) between WT and Tg rabbits at 12 weeks, but there was no significant difference (Table 1, Fig. 3). Next we compared the activity of cone OFF bipolar cells/horizontal cells between WT and Tg by measuring the change in the maximum a-wave after PDA. The degree of amplitude reduction of the a-wave after PDA in Tg was not significantly different from that of WT (see also the Appendix). Finally, we also found that the changes in the photopic ERG b-wave by TTX were not different between Tg and WT rabbits. Thus, we could not detect any changes in the input from the ON/OFF bipolar cells in our Tg rabbits. We are currently planning to analyze functional changes in the ON/OFF bipolar cells of Tg rabbits in more details using the vector modeling of flicker ERG.[50]

What kinds of further studies are needed? First, we could not determine which of two types of retinal cells, amacrine cells or ganglion cells, were the main contributors to the supernormal OPs in Tg rabbits. To determine this, photopic OPs should be recorded from Tg rabbits several weeks after optic nerve section to exclude the contribution of retinal ganglion cells. Second, we did not determine the exact mechanism of the supernormal OPs in Tg rabbit. The possible hypotheses include; an increase in the number of inner retinal neurons after the photoreceptor degeneration,[51] changes in the feedback communications, changes in some type of humoral factors which are released from degenerating neurons or glia,[52] transformation of neural phenotypes in the inner retina, changes in the resistance associated with photoreceptor loss, or synaptic rewiring in the inner retinal neurons after the photoreceptor degeneration.[53–55] Further anatomic and functional studies using immunohistochemistry,[47] ultrastructure, or single-unit response recording[56] in the inner retinal neurons of Tg rabbits may add more information on the exact mechanism of this phenomenon.

Finally, the question arises as to whether similar ERG changes occur in patients with RP. We recently studied all

components of macular cone ERGs in patients with RP at relatively early stages[57] and noted that macular OPs were better preserved than the a- and b-waves. We also found that one patient with RP had supernormal macular OP amplitudes: surprisingly, her summed OP amplitude was larger than those of any of the 43 normal subjects (Fig. 4B in Ref. 57). These macular ERG data raise a possibility that similar secondary functional changes can occur in some patients with RP, at least in some retinal areas. These functional changes in the inner retina may have important implications for future treatment strategy for patients with RP including cell transplantation[58] and retinal prosthesis.[59]

APPENDIX

Fitting Model for the Cone a-Wave

In this study we used the a-wave fitting model of Hood and Birch[2] to evaluate rod and cone photoreceptor function. However, several pharmacologic experiments have indicated that the photopic a-wave includes a PDA-sensitive, postreceptoral component in primates.[60-62] We investigated the change in the a-wave amplitude before and after PDA in WT rabbits and found that the maximum a-wave amplitude decreased 13% to 25% after PDA ($n = 3$), suggesting that the activities of postreceptoral neurons significantly contribute to the cone a-wave in rabbits. Thus, we assumed that in the method of OP extraction, the component of not only the cone photoreceptors, but also the component of OFF bipolar cell/horizontal cells were subtracted. In addition, we also supposed that when the Michaelis-Menten fit to the b-wave amplitude measurements was used, the ON bipolar cell component was mainly analyzed, since the negative component (some combination of cone and OFF cone bipolar/horizontal cell component) has been already subtracted.

Recently, Hood and Birch[63] have shown that the cone a-wave is better fitted with a filtered version of equation 1 in humans. They showed that a Michaelis-Menten version of the equation gives a better fit to the cone a-wave.

Amplitude Reduction of Photopic a-Wave of Tg Rabbits

One question regarding the reduction in the photopic a-wave in young Tg rabbits is whether this reduction is a reflection of cone contributions to the photopic ERG or whether it is a reduction in the OFF bipolar/horizontal cell component. We compared the effect of PDA on the maximum a-wave amplitude between WT and Tg rabbits at 16 weeks and found that the degree of amplitude reduction after PDA did not differ between WT (6.4 - 0.5 μV, $n = 3$) and Tg (6.1-7.5 μV, $n = 3$; $P = 0.23$). These results indicate that the amplitude reduction of the photopic a-wave of young Tg rabbits is mainly due to the decreased cone photoreceptor activity.

Acknowledgments

The authors thank Paul A. Sieving (National Eye Institute), Yozo Miyake (Shukutoku University), Michael A. Sandberg (Massachusetts Eye and Ear Infirmary), and Duco I. Hamasaki (Bascom Palmer Eye Institute) for critical comments and the anonymous reviewers for valuable suggestions.

References

1. Berson EL. Retinitis pigmentosa. The Friedenwald Lecture. *Invest Ophthalmol Vis Sci.* 1993;34:1659-1676.
2. Hood DC, Birch DG. Rod phototransduction in retinitis pigmentosa: estimation and interpretation of parameters derived from the rod a-wave. *Invest Ophthalmol Vis Sci.* 1994;35:2948-2961.
3. Shady S, Hood DC, Birch DG. Rod phototransduction in retinitis pigmentosa: distinguishing alternative mechanisms of degeneration. *Invest Ophthalmol Vis Sci.* 1995;36:1027-1037.
4. Cideciyan AV, Hood DC, Huang Y, et al. Disease sequence from mutant rhodopsin allele to rod and cone photoreceptor degeneration in man. *Proc Natl Acad Sci U S A.* 1998;95:7103-7108.
5. Kennan A, Aherne A, Humphries P. Light in retinitis pigmentosa. *Trends Genet.* 2005;21:103-110.
6. Hartong DT, Berson EL, Dryja TP. Retinitis pigmentosa. *Lancet.* 2006;368:1795-1809.
7. Daiger SP, Bowne SJ, Sullivan LS. Perspective on genes and mutations causing retinitis pigmentosa. *Arch Ophthalmol.* 2007;125:151-158.
8. Birch DG, Sandberg MA. Dependence of cone b-wave implicit time on rod amplitude in retinitis pigmentosa. *Vision Res.* 1987;27:1105-1112.
9. Cideciyan AV, Jacobson SG. Negative electroretinograms in retinitis pigmentosa. *Invest Ophthalmol Vis Sci.* 1993;34:3253-3263.
10. Hood DC, Birch DG. Abnormalities of the retinal cone system in retinitis pigmentosa. *Vision Res.* 1996;36:1699-1709.
11. Falsini B, Iarossi G, Porciatti V, et al. Postreceptoral contribution to macular dysfunction in retinitis pigmentosa. *Invest Ophthalmol Vis Sci.* 1994;35:4282-4290.
12. Machida S, Kondo M, Jamison JA, et al. P23H rhodopsin transgenic rat: correlation of retinal function with histopathology. *Invest Ophthalmol Vis Sci.* 2000;41:3200-3209.
13. Aleman TS, LaVail MM, Montemayor R, et al. Augmented rod bipolar cell function in partial receptor loss: an ERG study in P23H rhodopsin transgenic and aging normal rats. *Vision Res.* 2001;41:2779-2797.
14. Ueno S, Kondo M, Miyata K, et al. Physiological function of S-cone system is not enhanced in rd7 mice. *Exp Eye Res.* 2005;81:751-758.
15. Bush RA, Hawks KW, Sieving PA. Preservation of inner retinal responses in the aged Royal College of Surgeons rat: evidence against glutamate excitotoxicity in photoreceptor degeneration. *Invest Ophthalmol Vis Sci.* 1995;36:2054-2062.
16. Machida S, Raz-Prag D, Fariss RN, et al. Photopic ERG negative response from amacrine cell signaling in RCS rat retinal degeneration. *Invest Ophthalmol Vis Sci.* 2008;49:442-452.
17. Banin E, Cideciyan AV, Alemán TS, et al. Retinal rod photoreceptor-specific gene mutation perturbs cone pathway development. *Neuron.* 1999;23:549-557.
18. Kondo M, Sakai T, Komeima K, et al. Generation of a transgenic rabbit model of retinal degeneration. *Invest Ophthalmol Vis Sci.* 2009;50:1371-1377.
19. Oh KT, Longmuir R, Oh DM, et al. Comparison of the clinical expression of retinitis pigmentosa associated with rhodopsin mutations at codon 347 and codon 23. *Am J Ophthalmol.* 2003;136:306-313.
20. Berson EL, Rosner B, Sandberg MA, et al. Ocular findings in patients with autosomal dominant retinitis pigmentosa and rhodopsin, proline-347-leucine. *Am J Ophthalmol.* 1991;111:614-623.
21. Wachtmeister L. Oscillatory potentials in the retina: what do they reveal. *Prog Retin Eye Res.* 1998;17:485-521.
22. Dong CJ, Agey P, Hare WA. Origins of the electroretinogram oscillatory potentials in the rabbit retina. *Vis Neurosci.* 2004;21:533-543.
23. Zhang K, Yao G, Gao Y, et al. Frequency spectrum and amplitude analysis of dark- and light-adapted oscillatory potentials in albino mouse, rat and rabbit. *Doc Ophthalmol.* 2007;115:85-93.
24. Rangaswamy NV, Hood DC, Frishman LJ. Regional variations in local contributions to the primate photopic flash ERG: revealed using the slow-sequence mfERG. *Invest Ophthalmol Vis Sci.* 2003;44:3233-3247.
25. Forte JD, Bui BV, Vingrys AJ. Wavelet analysis reveals dynamics of rat oscillatory potentials. *J Neurosci Methods.* 2008;169:191-200.
26. Yang XW, Model P, Heintz N. Homologous recombination based modification in Escherichia coli and germline transmission in trans-

genic mice of a bacterial artificial chromosome. *Nat Biotechnol.* 1997;15:859-865.

27. Zhang Y, Buchholz F, Muyrers JP, Stewart AF. A new logic for DNA engineering using recombination in Escherichia coli. *Nat Genet.* 1998;20:123-128.
28. Muyrers JP, Zhang Y, BenesV, et al. Point mutation of bacterial artificial chromosomes by ET recombination. *EMBO Rep.* 2000;1: 239-243.
29. Lamb TD, Pugh EN Jr. A quantitative account of the activation steps involved in phototransduction in amphibian photoreceptors. *J Physiol.* 1992;449:719-758.
30. Fulton AB, Rushton WA. The human rod ERG: correlation with psychophysical responses in light and dark adaptation. *Vision Res.* 1978;18:793-800.
31. Robson JG, Frishman LJ. Response linearity and kinetics of the cat retina: the bipolar cell component of the dark-adapted electroretinogram. *Vis Neurosci.* 1995;12:837-850.
32. Akula JD, Mocko JA, Moskowitz A, et al. The oscillatory potentials of the dark-adapted electroretinogram in retinopathy of prematurity. *Invest Ophthalmol Vis Sci.* 2007;48:5788-5797.
33. Sieving PA, Murayama K, Naarendorp F. Push-pull model of the primate photopic electroretinogram: a role for hyperpolarizing neurons in shaping the b-wave. *Vis Neurosci.* 1994;11:519-532.
34. Ueno S, Kondo M, Ueno M, et al. Contribution of retinal neurons to d-wave of primate photopic electroretinograms. *Vision Res.* 2006;46:658-664.
35. Kondo M, Kurimoto Y, Sakai T, et al. Recording focal macular photopic negative response (PhNR) from monkeys. *Invest Ophthalmol Vis Sci.* 2008;49:3544-3550.
36. Lachapelle P, Little JM, Polomeno RC. The photopic electroretinogram in congenital stationary night blindness with myopia. *Invest Ophthalmol Vis Sci.* 1983;24:442-450.
37. Slaughter MM, Miller RF. 2-amino-4-phosphonobutyric acid: a new pharmacological tool for retina research. *Science.* 1981;211:182-185.
38. Guité P, Lachapelle P. The effect of 2-amino-4-phosphonobutyric acid on the oscillatory potentials of the electroretinogram. *Doc Ophthalmol.* 1990;75:125-133.
39. Hare WA, Ton H. Effects of APB, PDA, and TTX on ERG responses recorded using both multifocal and conventional methods in monkey: effects of APB, PDA, and TTX on monkey ERG responses. *Doc Ophthalmol.* 2002;105:189-222.
40. Slaughter MM, Miller RF. An excitatory amino acid antagonist blocks cone input to sign-conserving second-order retinal neurons. *Science.* 1983;219:1230-1232.
41. Naarendorp F, Sieving PA. The scotopic threshold response of the cat ERG is suppressed selectively by GABA and glycine. *Vision Res.* 1991;31:1-15.
42. Narahashi T, Moore JW, Scott WR. Tetrodotoxin blockage of sodium conductance increase in lobster giant axons. *J Gen Physiol.* 1964;47:965-974.
43. Bloomfield SA. Effect of spike blockade on the receptive-field size of amacrine and ganglion cells in the rabbit retina. *J Neurophysiol.* 1996;75:1878-1893.
44. Stafford DK, Dacey DM. Physiology of the A1 amacrine: a spiking, axon-bearing interneuron of the macaque monkey retina. *Vis Neurosci.* 1997;14:507-522.
45. Viswanathan S, Frishman LJ, Robson JG, et al. The photopic negative response of the macaque electroretinogram: Reduction by experimental glaucoma. *Invest Ophthalmol Vis Sci.* 1999;40: 1124-1136.
46. Bui BV, Fortune B. Ganglion cell contributions to the rat full-field electroretinogram. *J Physiol.* 2004;555:153-173.
47. Mojumder DK, Frishman LJ, Otteson DC, Sherry DM. Voltage-gated sodium channel alpha-subunits Na(v)1.1, Na(v)12, and Na(v)16 in the distal mammalian retina. *Mol Vis.* 2007;13:2163-2182.
48. Mojumder DK, Sherry DM, Frishman LJ. Contribution of voltage-gated sodium channels to the b-wave of the mammalian flash electroretinogram. *J Physiol.* 2008;586:2551-2580.
49. Hood DC, Birch DG. A computational model of the amplitude and implicit time of the b-wave of the human ERG. *Vis Neurosci.* 1992;8:107-126.
50. Kondo M, Sieving PA. Primate photopic sine-wave flicker ERG: vector modeling analysis of component origins using glutamate analogs. *Invest Ophthalmol Vis Sci.* 2001;42:305-312.
51. Beltran WA, Hammond P, Acland GM, Aguirre GD. A frameshift mutation in RPGR exon ORF15 causes photoreceptor degeneration and inner retina remodeling in a model of X-linked retinitis pigmentosa. *Invest Ophthalmol Vis Sci.* 2006;47:1669-1681.
52. Hankins M, Ikeda H. Early abnormalities of retinal dopamine pathways in rats with hereditary retinal dystrophy. *Doc Ophthalmol.* 1994;86:325-334.
53. Marc RE, Jones BW, Watt CB, Strettoi E. Neural remodeling in retinal degeneration. *Prog Retin Eye Res.* 2003;22:607-655.
54. Marc RE, Jones BW, Anderson JR, et al. Neural reprogramming in retinal degeneration. *Invest Ophthalmol Vis Sci.* 2007;48:3364-3371.
55. Peng YW, Hao Y, Petters RM, Wong F. Ectopic synaptogenesis in the mammalian retina caused by rod photoreceptor-specific mutations. *Nat Neurosci.* 2000;3:1121-1127.
56. Pu M, Xu L, Zhang H. Visual response properties of retinal ganglion cells in the royal college of surgeons dystrophic rat. *Invest Ophthalmol Vis Sci.* 2006;47:3579-4585.
57. Ikenoya K, Kondo M, Piao CH, et al. Preservation of macular oscillatory potentials in eyes of patients with retinitis pigmentosa and normal visual acuity. *Invest Ophthalmol Vis Sci.* 2007;48: 3312-3317.
58. MacLaren RE, Pearson RA, MacNeil A, et al. Retinal repair by transplantation of photoreceptor precursors. *Nature.* 2006;444: 203-207.
59. Weiland JD, Liu W, Humayun MS. Retinal prosthesis. *Annu Rev Biomed Eng.* 2005;7:361-401.
60. Bush RA, Sieving PA. A proximal retinal component in the primate photopic ERG a-wave. *Invest Ophthalmol Vis Sci.* 1994;35:635-645.
61. Jamison JA, Bush RA, Lei B, Sieving PA. Characterization of the rod photoresponse isolated from the dark-adapted primate ERG. *Vis Neurosci.* 2001;18:445-455.
62. Robson JG, Saszik SM, Ahmed J, Frishman LJ. Rod and cone contributions to the a-wave of the electroretinogram of the macaque. *J Physiol.* 2003;547:509-530.
63. Hood DC, Birch DG. Measuring the health of the human photoreceptors with the leading edge of the a-wave. In: Heckenlively JR, Arden GB, eds. *Principles and Practice of Clinical Electrophysiology of Vision.* 2nd ed. Cambridge, MA: The MIT Press; 2006: 487-501.

Experimental Eye Research 88 (2009) 92–98

Contents lists available at ScienceDirect

Experimental Eye Research

journal homepage: www.elsevier.com/locate/yexer

Asymmetry of focal macular photopic negative responses (PhNRs) in monkeys

Yukihide Kurimoto [a], Mineo Kondo [a,*], Shinji Ueno [a], Takao Sakai [a], Shigeki Machida [b], Hiroko Terasaki [a]

[a] Department of Ophthalmology, Nagoya University Graduate School of Medicine, 65 Tsuruma-cho, Showa-ku, Nagoya 466-8550, Japan
[b] Department of Ophthalmology, Iwate Medical University School of Medicine, Morioka, Japan

ARTICLE INFO

Article history:
Received 26 August 2008
Accepted in revised form 15 October 2008
Available online 1 November 2008

Keywords:
electroretinogram
photopic negative response (PhNR)
asymmetry
macula
focal
monkey

ABSTRACT

The photopic negative response (PhNR) is a slow, negative-going wave of the photopic electroretinogram (ERG) that appears after the b-wave. Recent studies have shown that the PhNR originates from the spiking activities of inner retinal neurons including the ganglion cells and their axons. The aim of this study was to determine whether there is any asymmetry in the amplitude of the PhNR elicited from the upper and lower macular areas, and between the nasal and temporal macular areas in rhesus monkeys. To accomplish this, we recorded focal macular PhNRs that were elicited by red hemi-circular stimuli presented on a blue background. We show that the PhNR from the upper macular area was significantly larger than that of the lower macular area, and the PhNR of the nasal macula was significantly larger than that of the temporal macula. These asymmetries were present in the focal PhNR elicited by both brief and long duration stimuli, and the asymmetries were completely eliminated by an intravitreal injection of tetrodotoxin (TTX). These results suggest that the upper–lower and nasal-temporal asymmetries of PhNR in the primate retina are mainly caused by TTX-sensitive spiking activities of inner retinal neurons.

1. Introduction

The photopic negative response (PhNR) is a slow, negative-going wave of the photopic electroretinogram (ERG) that appears after the b-wave. Studies by Frishman and colleagues have demonstrated that the PhNR originates from the spiking activity of inner retinal neurons including the retinal ganglion cells and their axons (Rangaswamy et al., 2007; Viswanathan et al., 1999, 2000).The PhNR has been used in clinical studies to evaluate the inner retinal function objectively in several diseases, including glaucoma (Colotto et al., 2000; Drasdo et al., 2001; Machida et al., 2008; Viswanathan et al., 2001), optic nerve diseases (Gotoh et al., 2004; Miyata et al., 2007; Rangaswamy et al., 2004), and retinal vascular diseases (Chen et al., 2006; Kizawa et al., 2006; Machida et al., 2004). In these studies, the PhNRs were elicited mainly by full-field stimuli, and there have been only a few studies where the PhNR were elicited from localized retinal areas (Clotto et al., 2000; Fortune et al., 2003; Viswanathan et al., 2000). In addition, there have been only two studies of the focal PhNR with simultaneous fundus monitoring (Kondo et al., 2008; Machida et al., 2008).

We have recently developed a new recording system of focal PhNR (Kondo et al., 2008), which was modified from Miyake et al., 1988. In this system, the examiner can monitor the position of the stimulus spot on the fundus precisely during the recordings. In addition, a red stimulus spot was used on a blue background illumination, because a recent study showed that this color combination was most effective in eliciting large PhNRs especially for weak to moderate stimulus intensities (Rangaswamy et al., 2007). With this system, we found that the amplitude of the PhNR of the focal ERG was relatively large in the macular area (Kondo et al., 2008). However, we did not examine whether there were any regional variations or asymmetry in the amplitude of the PhNR in the macular area of monkeys. We believe that when the focal macular PhNRs are recorded from normal and diseased retinas, it is important to know whether there are any regional variations or asymmetries in the focal macular PhNR.

Thus, the purpose of this study was to determine whether the focal PhNRs recorded from the upper and lower macular areas, and nasal and temporal macular areas using a hemi-circular stimulus were symmetrical. We show that there were distinct asymmetries of the PhNR amplitude in both the vertical and horizontal directions in monkeys. We examined how these asymmetries of the focal PhNR change after the spiking activities of the inner retinal neurons are blocked by an intravitreal injection of tetrodotoxin (TTX) in monkeys.

2. Methods

2.1. Animals

Five eyes of five rhesus monkeys (*Macaca mulata*) were studied. The animals were sedated with an intramuscular injection of

* Corresponding author. Tel.: +81 52 744 2271; fax: +81 52 744 2278.
E-mail address: kondomi@med.nagoya-u.ac.jp (M. Kondo).

0014-4835/$ – see front matter © 2008 Elsevier Ltd. All rights reserved.
doi:10.1016/j.exer.2008.10.012

ketamine hydrochloride (7 mg/kg initial dose; 5–10 mg/kg per h maintenance dose) and xylazine (0.6 mg/kg). The respiration and heart rate were monitored, and hydration was maintained with slow infusion of lactated Ringer solution. The cornea was anesthetized with topical 1% tetracaine, and the pupils dilated with topical 0.5% tropicamide, 0.5% phenylephrine HCl, and 1% atropine. All experimental and animal care procedures adhered to the ARVO Statement for the Use of Animals in Ophthalmic and Vision Research, and were approved by the Institutional Animal Care Committee of the Nagoya University.

2.2. Stimulus and observation system

Our system for recording focal PhNRs has been described in detail (Kondo et al., 2008). Briefly, an infrared fundus camera was modified to observe the fundus and stimulate the retina. Light emitting diodes (LEDs) were incorporated into the camera to be used for the stimulus and background illuminations. The infrared television fundus camera (Kowa VX-10, Tokyo, Japan) was modified to obtain a Maxwellian stimulating system. The image from this fundus camera was fed to a television monitor with a 45° view of the posterior pole of the eye. The position of the stimulus spot on the fundus could be moved by the examiner with a joystick, and the position was monitored on the television monitor (Fig. 1, upper trace).

A red LED ($\lambda_{max} = 627$ nm; LXK2-PD12-S00, Philips Lumileds, San Jose, CA, USA) was used as the stimulus source, and a blue LED ($\lambda_{max} = 450$ nm; L450, Epitex, Kyoto, Japan) was used for the background illumination that covered a retinal area of 45°. A hemi-circular red stimulus (15° in diameter) was used (Fig. 1, lower trace).

The luminance of blue background was fixed at 100 scot cd/m^2, which is known to be high enough to suppress the rod photoreceptors. The luminance of the red stimulus spot was 55 phot cd/m^2, and the stimulus durations were 10 and 150 ms. We have already shown that the responses recorded with this system were focal when the luminance of the red stimulus spot was $\leq$55 phot cd/m^2 and presented on a steady blue background of 100 scot cd/m^2 (Kondo et al., 2008). The strength of the brief flashes of 10 ms was 0.55 phot cd-s/m^2 in energy units. The stimulus repetition rate was fixed at 2 Hz.

The luminances of the stimulus and background were measured at the position of corneal surface, and then converted to the value at the retinal surface. These luminances were measured with a photometer (Model IL 1700; International Light, Newburyport, MA, USA).

2.3. Recording and analyses

ERGs were picked-up with a Burian-Allen bipolar contact lens electrode (Hansen Ophthalmic Development Labs, Iowa City, USA), and the ground electrode was attached to the ipsilateral ear. The responses were amplified, and the band pass filters were set at 0.5 and 1000 Hz. The ERGs were digitized at 5 kHz, and 100– 300 responses were averaged for each response (MEB-9100, Neuropack, Nihon Kohden, Tokyo, Japan).

The amplitude of the PhNR was measured from the baseline to the bottom of the negative trough after the b-wave for the brief flashes of 10 ms, or was measured from the positive peak of the b-wave to the negative trough after the b-wave for the long duration

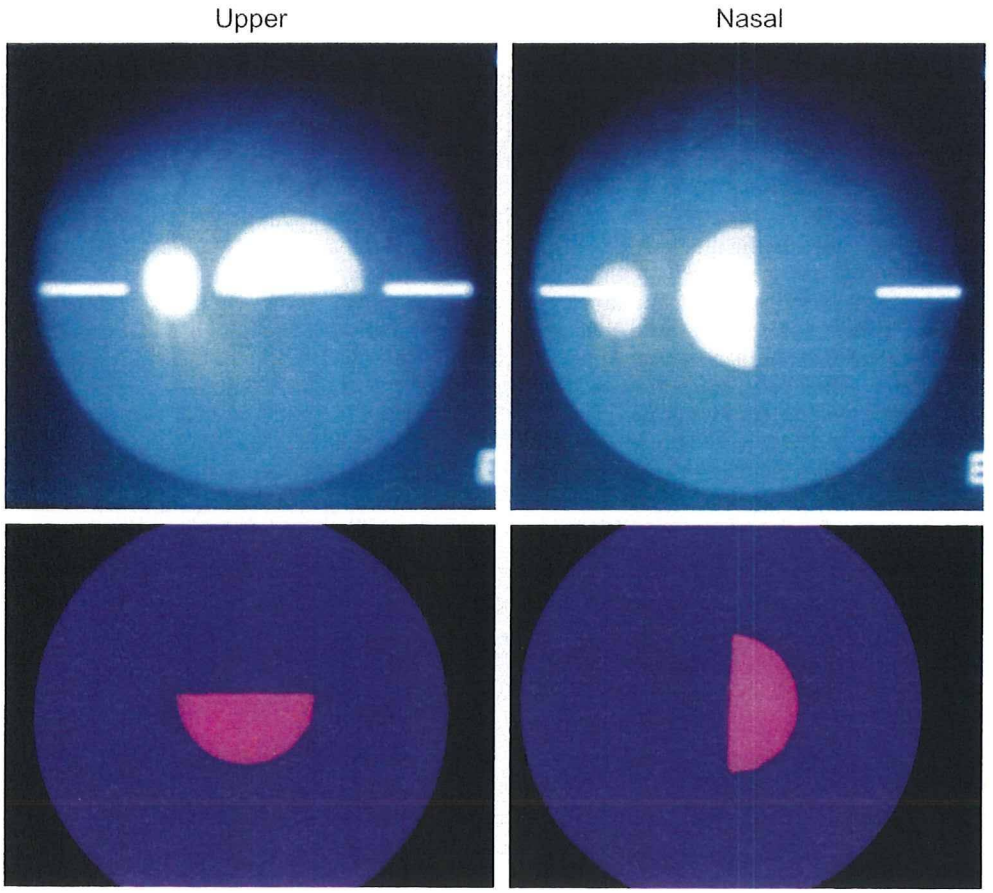

Fig. 1. Stimulus configuration for stimulating localized areas of the macula. Upper trace: Infrared fundus image of the monkey retina. The 15° hemi-circular stimulus is positioned on the upper (left) and nasal macula (right) of a rhesus monkey. Lower trace: Image of the red stimulus spot on the blue background. This image was photographed by a digital camera at the position of monkey's eye.

flashes of 150 ms as done in previous studies (Rangaswamy et al., 2007; Viswanathan et al., 1999). The amplitudes of the a- and b-waves were measured from the baseline to the first negative trough and from the negative trough to the next positive peak, respectively.

2.4. Injection of tetrodotoxin (TTX)

The intravitreal injection techniques have been described in detail (Hood et al., 1999; Kondo et al., 2008; Ueno et al., 2004, 2006; Viswanathan et al., 1999). The TTX was injected into the vitreous with a 30-gauge needle inserted through the pars plana approximately 3 mm posterior to the limbus. The TTX (Kanto Chemical, Tokyo Japan) was dissolved in sterile saline, and 0.05– 0.07 ml was injected. The intravitreal concentrations of TTX was 4 μM assuming that the monkey's vitreous volume is 2.1 ml.

Because the effect of TTX is maximal at about 60 min after the drug injection, recordings were begun about 60 min after the injections, and studies were completed within 3 h. The results that are shown were recorded from eyes not previously treated.

2.5. Statistical analyses

The data were analyzed with the Stat View ver.5 computer software. The amplitude of each ERG component (a-wave, b-wave, and PhNR) from the upper and lower macular areas, or from the nasal and temporal macular areas were compared using paired t -tests. A difference was considered statistically significant when $P < 0.05$.

3. Results

3.1. Asymmetry between upper and lower macular areas

Representative focal macular ERGs recorded from upper and lower macula areas in a rhesus monkey (monkey #4) are shown in Fig. 2A. The focal ERGs for brief-flashes (10 ms) and long-flashes (150 ms) are presented in the upper and lower traces, respectively. At first glance, the focal ERGs from the upper and lower macula areas appear nearly the same. But when the two waveforms were superimposed, the amplitude of the PhNR was slightly larger in the upper macular than in the lower macular areas for both brief and long duration stimuli (right most column of Fig. 2A).

The amplitudes of the PhNRs recorded from upper and lower macular areas for five different animals are plotted in Fig. 2B. The amplitudes from the upper macular area were larger than that recorded from the lower macular area in all five animals, although there was a large variation in the PhNR amplitude among the five animals. The mean (±SEM) PhNR amplitude of the upper macular area was 3.3 ± 0.4 μV which was 27% larger than that of lower macula at 2.6 ± 0.4 μV for brief-flashes ($P < 0.05$). Similarly, the mean (±SEM) PhNR amplitude of the upper retina was 5.4 ± 0.7 μV which was 20% larger than that of lower retina at 4.5 ± 0.5 μV for long duration stimuli ($P < 0.01$).

The mean (±SEM) of the amplitudes for the a-wave, b-wave, and PhNR are plotted in Fig. 2C. We noted that not only the PhNR amplitude, but also the a-wave amplitude was significantly larger in the upper macula than in the lower macula for brief-flashes ($P < 0.05$).

3.2. Asymmetry of PhNR recorded from nasal and temporal macular areas

Representative focal macular ERGs recorded from nasal and temporal retinas in the same monkey shown in Fig. 2A (monkey #4) are shown in Fig. 3A. We found that the amplitude of the PhNR recorded from the nasal macular area was slightly larger than the PhNR of temporal macular area for both brief and long duration stimuli in all five animals (Fig. 3B). For short duration stimuli, the mean (±SEM) PhNR amplitude of the nasal macular area was 3.3 ± 0.4 μV, which was 27% larger than that of temporal macular

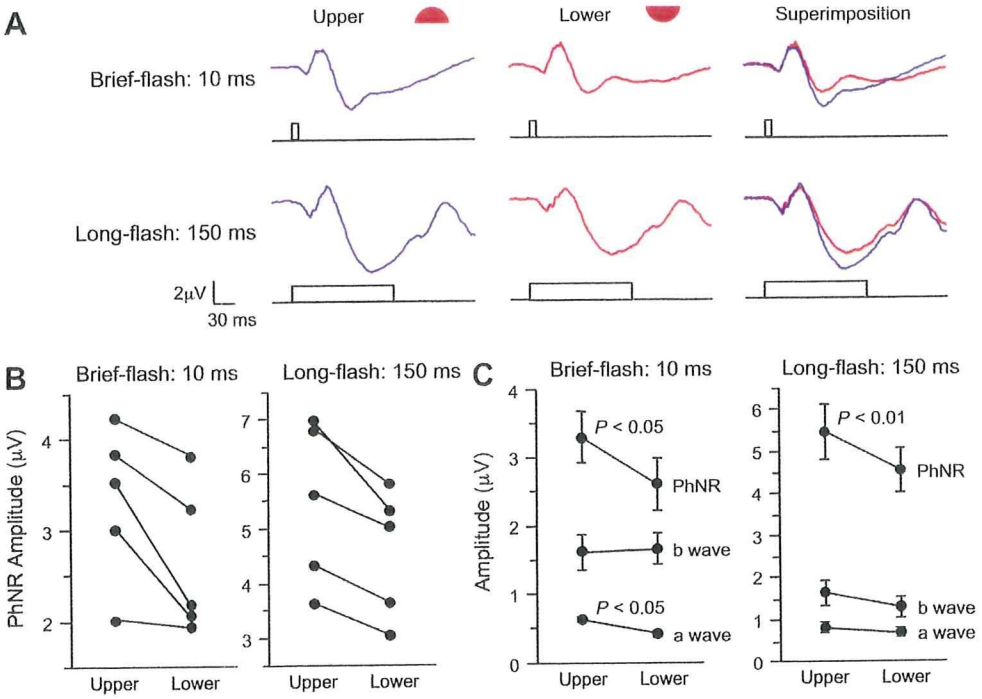

Fig. 2. Focal macular ERGs. (A) Representative focal macular ERGs recorded from the upper and lower macular areas in a rhesus monkey. ERGs for short duration (10 ms) and long duration (150 ms) stimuli are presented in the upper and lower traces, respectively. (B) Plot of the PhNR amplitude from five different monkeys. (C) Mean (±SEM) of the amplitudes for the a-wave, b-wave, and PhNR recorded from upper and lower macular areas for five monkeys. Note that the PhNR of upper macula is significantly larger than that of the lower macula.

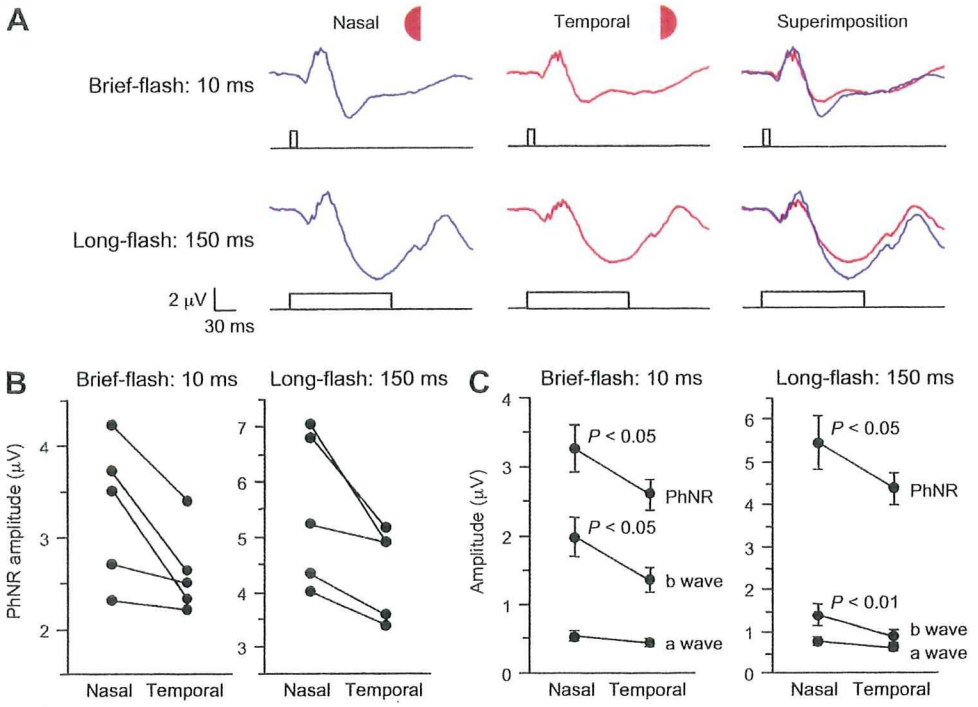

Fig. 3. Focal macular ERGs recorded from the nasal and temporal macular areas. (A) Representative focal macular ERGs recorded from nasal and temporal macular areas in a rhesus monkey. ERGs for short duration (10 ms) and long duration (150 ms) stimuli are presented in the upper and lower traces, respectively. (B) Plot of the PhNR amplitudes from five different monkeys. (C) Mean (±SEM) of the amplitudes for the a-wave, b-wave, and PhNR recorded from nasal and temporal maculae for five monkeys. Note that the PhNR of nasal macula is significantly larger than that of temporal macula.

area at 2.6 ± 0.2 μV. For long duration stimuli, the mean (±SEM) PhNR amplitude of the nasal macular area was 5.5 ± 0.6 μV which was 25% larger than that of temporal macular area at 4.4 ± 0.4 μV. All of these differences were statistically significant ($P < 0.05$).

The mean (±SEM) of the amplitudes for a-wave, b-wave, and PhNR are plotted in Fig. 3C. Not only the PhNR, but the b-wave was also significantly larger in the nasal macula than in the temporal macula for both short and long duration stimuli ($P < 0.05$).

3.3. *Effect of TTX on upper–lower asymmetry*

We next wanted to determine how TTX-sensitive neural activities contributed to the asymmetry of PhNR in monkeys. For this, we recorded the focal macular ERGs from different retinal locations before and after an intravitreal injection of TTX in two monkeys. Focal macular ERGs recorded from the upper and lower macular area before and after an intravitreous injection of TTX from a monkey (#4) are shown in Fig. 4A. As shown in Fig. 2, the PhNR amplitude was slightly larger in the upper macula than in the lower macula before the TTX injection (black waveforms). After the injection of TTX, the amplitudes of PhNR were greatly reduced for both short and long duration stimuli (blue and red waveforms).

The component removed by the TTX was isolated by subtracting the post-TTX response from the pre-TTX response (green and orange waveform). We found that the amplitude of TTX-sensitive negative component was 55 and 33% larger in the upper macula than in the lower macula for both short and long duration stimuli, respectively (third column from the left). In another monkey (monkey #5), the amplitude of this TTX-sensitive negative component was 35 and 23% larger in the upper macular area than in the lower macular area for both brief and long-flashes, respectively (Fig. 4B).

Interestingly, waveforms of the remaining ERGs after TTX from upper and lower areas became identical (second column from the left of Fig. 4A). This was also true for another animal (monkey #5, blue and red waveforms of Fig. 4B).

3.4. *Effect of TTX on nasal-temporal asymmetry*

We also studied the effect of TTX on the nasal-temporal asymmetry of the PhNR in two monkeys. Focal macular ERGs recorded from the nasal and temporal macular areas before and after intravitreal TTX injection (monkey #4) are shown in Fig. 5A. As in Fig. 4, the amplitudes of PhNR were greatly reduced after the TTX injection for both short and long duration stimuli.

The component removed by TTX was isolated by subtracting the post-TTX response from the pre-TTX response. We found that the amplitude of the TTX-sensitive negative component was 42 and 31% larger in the nasal macula than in the temporal macula for both short and long duration stimuli, respectively (third column from the left). In another monkey (monkey #5), the amplitude of TTX-sensitive negative component was 23 and 22% larger in the nasal macula than in the temporal macula for both sort and long duration stimuli, respectively (Fig. 5B).

Again, waveforms of the remaining ERGs after TTX from nasal and temporal areas became identical (second column from the left of Fig. 5A), and overlapped for two monkeys (second column from the left of Fig. 5A, and blue and red waveforms of Fig. 5B).

4. Discussion

Our results demonstrated that there were significant asymmetries in the amplitude of PhNR in the macular area of monkeys. The PhNR of upper macula was larger than that of lower macula, and the PhNR of nasal macula was larger than that of temporal macula. These asymmetries of the PhNR were present for both short and long duration stimuli. The degree of the differences in the PhNR amplitude was dependent on the stimulus duration and locations, and ranged from 20 to 27% for the stimuli used in this study. To the

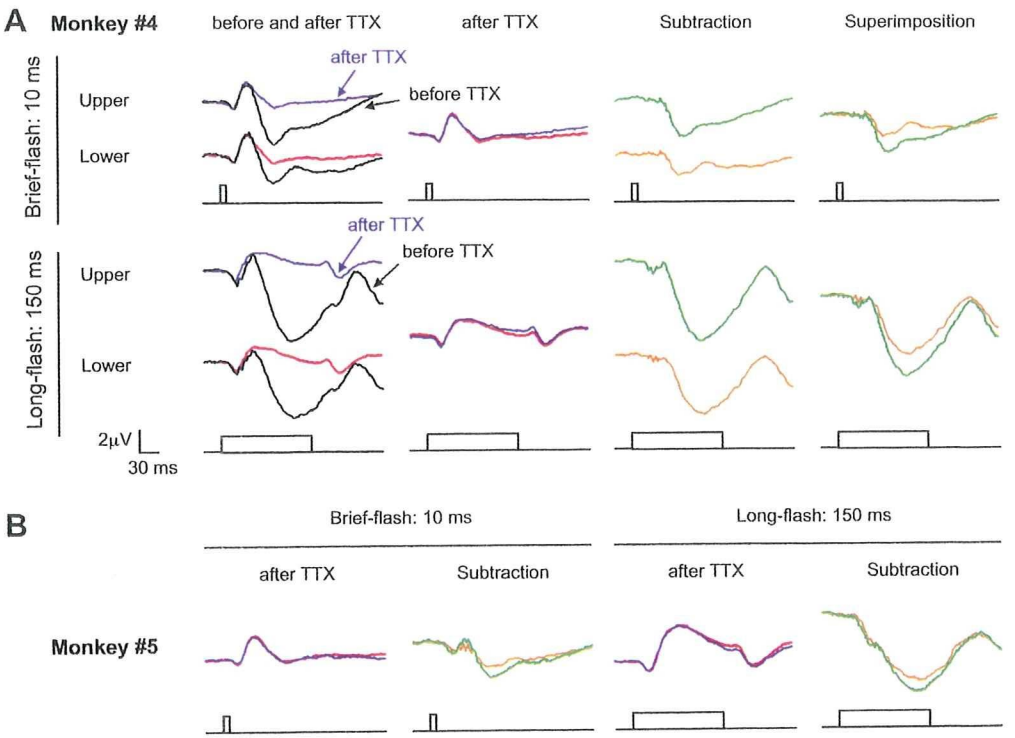

Fig. 4. Effect of tetrodotoxin (TTX) on the PhNR. (A) Representative focal ERGs recorded from the upper and lower macular areas before and after an intravitreal injection of TTX in a monkey (#4). ERGs elicited by short duration stimuli are shown in the upper trace, and ERGs elicited by long duration stimuli are shown in the lower traces. Subtracted TTX-sensitive components are also shown in the third and fourth rows from the left. (B) Results from another monkey (#5). Waveforms after TTX and subtracted TTX-sensitive components from upper and lower maculae are superimposed.

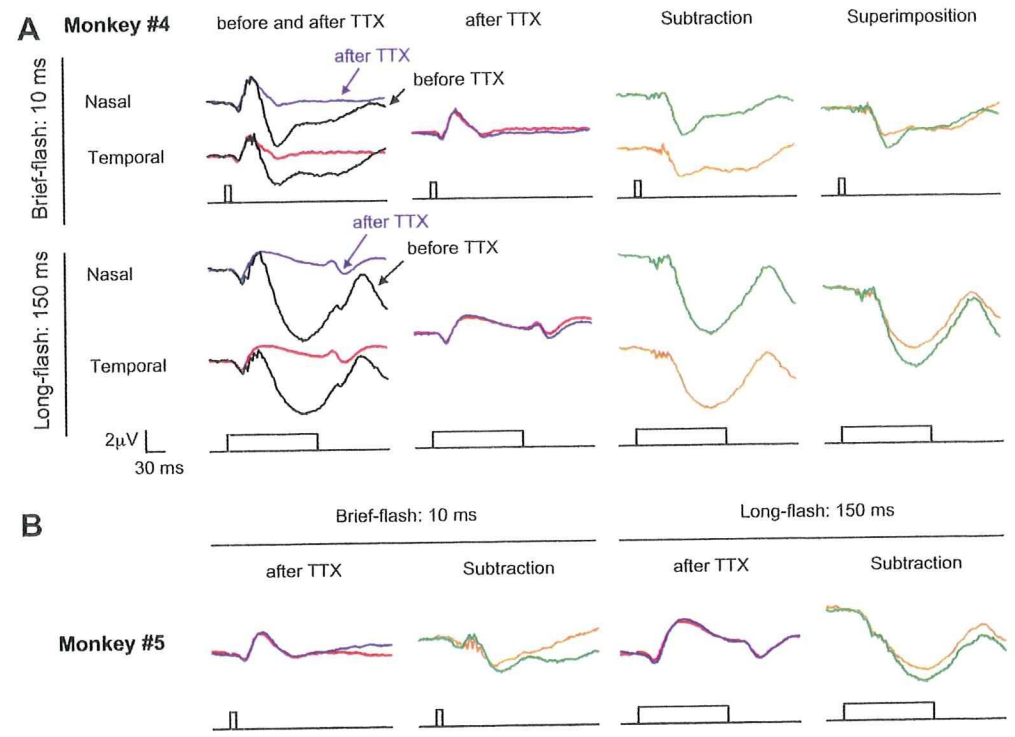

Fig. 5. Effect of tetrodotoxin (TTX) on the PhNR. (A) Representative focal ERGs recorded from the nasal and temporal macular areas before and after intravitreal injection of TTX in monkey #4. The ERGs to short duration stimuli are shown in the upper traces, and ERGs to long duration stimuli are shown in the lower traces. The subtracted TTX-sensitive components are shown in the third and fourth rows from the left. (B) Results from another monkey (#5). Waveforms after TTX and subtracted TTX-sensitive components from nasal and temporal maculae are superimposed.

best of our knowledge, this is the first demonstration that there is upper–lower and nasal-temporal asymmetries of the PhNR amplitudes in primates.

The asymmetries in the amplitudes were observed not only in the PhNR but also in the a- and b-waves of the focal macular ERGs (Figs. 2 and 3). One question then arises as to whether the larger PhNRs in the superior and nasal macular areas may be due to the larger signal inputs transmitted to the inner retina. To exclude this possibility, we blocked the spiking activities of inner retinal neurons by intravitreal injection of TTX. The results showed that after TTX, there was no apparent asymmetry in the waveforms of focal macular ERGs between the superior and inferior macular areas, and between nasal and temporal macular areas (Figs. 4 and 5). In contrast, subtracted TTX-sensitive components showed distinct upper–lower and nasal-temporal asymmetries. These findings were consistent for the two different monkeys tested. These results suggested that the larger PhNRs at the upper and nasal macular areas were not due to the larger signal inputs transmitted to the inner retinal neurons, but were mainly caused by TTX-sensitive spiking activity of inner retinal neurons.

Our results of asymmetry in the PhNR amplitude are in agreement with previous histological studies in humans (Curcio and Allen, 1990) and monkeys (Perry and Cowey, 1985; Silveira et al., 1989, 1993). They reported that the ganglion cell density of the upper retina is higher than that of lower retina, and ganglion cell density of nasal retina was higher than that of the temporal retina, including macular area. Curcio and Allen (1990) reported that the ganglion cell density is about 15% higher in the nasal retina than at equivalent eccentricities in temporal retina from 0.4 to 2.0 mm eccentricity in human retinas. They also found that the ganglion cell density is approximately equal between upper and lower retinas at the eccentricities of 0.4 –2 mm, but the upper retina has 65% higher ganglion cell density than inferior retina at eccentricities of 2 –4 mm. When we consider the size of a stimulus spot of 15°, which corresponds to a retinal area of 2.8– 3.0 mm from the fovea, it is reasonable to interpret that the asymmetry of PhNR amplitude found in this study was mainly caused by the asymmetry of ganglion cell density.

Our results are also in agreement with other electrophysiological studies. The amplitude of pattern ERG, which is also thought to reflect the activity of ganglion cells and axons (Baker et al., 1988; Maffei and Fiorentini, 1981; Maffei et al., 1985), was larger in the upper retina than in the lower retina (Graham et al., 1994; Yoshii and Päärmann, 1989). In addition, the amplitude of the pattern ERG was greater in the nasal retina than in the temporal retina (Bopp, 1982; Porrello and Falsini, 1999; Yoshii and Päärmann, 1989). These findings combined with a recent study comparing the PhNR and pattern ERG in monkeys (Viswanathan et al., 2000) supported the idea that the PhNR and pattern ERG may be of similar cellular origin.

It is known that another inner retinal ERG component, the oscillatory potentials (OPs), shows a distinct nasal-temporal asymmetry in the retina of humans (Bearse et al., 2000; Miyake et al., 1989; Wu and Sutter, 1995) and monkeys (Rangaswamy et al., 2003, 2006). In contrast to PhNR, the OPs are larger in the temporal retina than in the nasal retina. Recent studies found that this nasal-temporal asymmetry of OPs was greatly reduced in monkeys after an intravitreal injection of TTX (Rangaswamy et al., 2003), monkeys with experimental glaucoma (Rangaswamy et al., 2006), and patients with glaucoma (Fortune et al., 2002). This nasal-temporal asymmetry in OPs is thought to be related to summation or subtraction of an optic nerve head component (ONHC) with local retinal component, depending upon the distance of the local region stimulated from the optic nerve head (Bearse et al., 2000; Zhou et al., 2007).

Hood et al. (1999) also studied the variation in the waveforms of fast multifocal ERG in rhesus monkeys. They found that intravitreal injection of TTX eliminated the variation and asymmetry in the waveforms of fast multifocal ERG across the retina. From these results, they suggested that the waveform variation and asymmetry in the fast multifocal ERG are mainly caused by TTX-sensitive inner retinal neurons.

What is the clinical relevance of this study? The focal PhNR has been used to assess inner retinal function of local areas in clinical situations (Drasdo et al., 2001; Machida et al., 2008). In the clinic, the focal PhNR may be separately recorded from upper and lower retinas, or from nasal and temporal retinas in patients with optic nerve diseases or glaucoma. In such occasions, it is important to remember that there are asymmetries in the PhNR amplitude in normal subjects. Furthermore, investigations are needed to study how local PhNRs are affected and how the asymmetry of PhNR changes in clinical diseases.

Acknowledgements

We thank Professor Yozo Miyake of Shukutoku University and Professor Duco I. Hamasaki for discussions on the manuscript. We also thank Mr Masao Yoshikawa, Hideteka Kudo, and Ei-ichiro Nagasaka of Mayo Corporation for technical help. Grant support: Health Sciences Research Grants (H16-sensory-001) from the Ministry of Health, Labor and Welfare, Japan, and Ministry of Education, Culture, Science and Technology (no. 18591913 and 18390466). The authors have no proprietary interests.

References

Baker Jr., C.L., Hess, R.R., Olsen, B.T., Zrenner, E., 1988. Current source density analysis of linear and non-linear components of the primate electroretinogram. J. Physiol. 407, 155–176.
Bearse Jr., M.A., Shimada, Y., Sutter, E.E., 2000. Distribution of oscillatory components in the central retina. Doc. Ophthalmol. 100, 185–205.
Bopp, M., 1982. Predominance of the nasal hemiretina in the pattern electroretinogram of the human eye. Pflügers Arch. 392, 50.
Chen, H., Wu, D., Huang, S., Yan, H., 2006. The photopic negative response of the flash electroretinogram in retinal vein occlusion. Doc. Ophthalmol. 113, 53–59.
Colotto, A., Falsini, B., Salgarello, T., Iarossi, G., Galan, M.E., Scullica, L., 2000. Photopic negative response of the human ERG: losses associated with glaucomatous damage. Invest. Ophthalmol. Vis. Sci. 41, 2205–2211.
Curcio, C.A., Allen, K.A., 1990. Topography of ganglion cells in human retina. J. Comp. Neurol. 300, 5–25.
Drasdo, N., Aldebasi, Y.H., Chiti, Z., Mortlock, K.E., Morgan, J.E., North, R.V., 2001. The S-cone PhNR and pattern ERG in primary open angle glaucoma. Invest. Ophthalmol. Vis. Sci. 42, 1266–1272.
Fortune, B., Bearse Jr., M.A., Cioffi, G.A., Johnson, C.A., 2002. Selective loss of an oscillatory component from temporal retinal multifocal ERG responses in glaucoma. Invest. Ophthalmol. Vis. Sci. 43, 2638–2647.
Fortune, B., Wang, L., Bui, B.V., Cull, G., Dong, J., Cioffi, G.A., 2003. Local ganglion cell contributions to the macaque electroretinogram revealed by experimental nerve fiber layer bundle defect. Invest. Ophthalmol. Vis. Sci. 44, 4567–4579.
Gotoh, Y., Machida, S., Tazawa, Y., 2004. Selective loss of the photopic negative response in patients with optic nerve atrophy. Arch. Ophthalmol. 122, 341–346.
Graham, S.L., Wong, V.A., Drance, S.M., Mikelberg, F.S., 1994. Pattern electroretinograms from hemifields in normal subjects and patients with glaucoma. Invest. Ophthalmol. Vis. Sci. 35, 3347–3356.
Hood, D.C., Frishman, L.J., Viswanathan, S., Robson, J.G., Ahmed, J., 1999. Evidence for a ganglion cell contribution to the primate electroretinogram (ERG): effects of TTX on the multifocal ERG in macaque. Vis. Neurosci. 16, 411–416.
Kizawa, J., Machida, S., Kobayashi, T., Gotoh, Y., Kurosaka, D., 2006. Changes of oscillatory potentials and photopic negative response in patients with early diabetic retinopathy. Jpn. J. Ophthalmol. 50, 367–373.
Kondo, M., Kurimoto, Y., Sakai, T., Koyasu, T., Miyata, K., Ueno, S., Terasaki, H., 2008. Recording focal macular photopic negative response (PhNR) from monkeys. Invest. Ophthalmol. Vis. Sci. 49, 3544–3550.
Machida, S., Gotoh, Y., Tanaka, M., Tazawa, Y., 2004. Predominant loss of the photopic negative response in central retinal artery occlusion. Am. J. Ophthalmol. 137, 938–940.
Machida, S., Toba, Y., Ohtaki, A., Gotoh, Y., Kaneko, M., Kurosaka, D., 2008. Photopic negative response of focal electoretinograms in glaucomatous eyes. Invest. Ophthalmol. Vis. Sci. [Epub ahead of print].
Maffei, L., Fiorentini, A., 1981. Electroretinographic responses to alternating gratings before and after section of the optic nerve. Science 211, 953–955.
Maffei, L., Fiorentini, A., Bisti, S., Holländer, H., 1985. Pattern ERG in the monkey after section of the optic nerve. Exp. Brain. Res. 59, 423–425.

Miyake, Y., Shiroyama, N., Ota, I., Horiguchi, M., 1988. Oscillatory potentials in electroretinograms of the human macular region. Invest. Ophthalmol. Vis. Sci. 29, 1631–1635.

Miyake, Y., Shiroyama, N., Horiguchi, M., Ota, I., 1989. Asymmetry of focal ERG in human macular region. Invest. Ophthalmol. Vis. Sci. 30, 1743–1749.

Miyata, K., Nakamura, M., Kondo, M., Lin, J., Ueno, S., Miyake, Y., Terasaki, H., 2007. Reduction of oscillatory potentials and photopic negative response in patients with autosomal dominant optic atrophy with OPA1 mutations. Invest. Ophthalmol. Vis. Sci. 48, 820–824.

Perry, V.H., Cowey, A., 1985. The ganglion cell and cone distributions in the monkey's retina: implications for central magnification factors. Vision Res. 25, 1795–1810.

Porrello, G., Falsini, B., 1999. Retinal ganglion cell dysfunction in humans following post-geniculate lesions: specific spatio-temporal losses revealed by pattern ERG. Vision Res. 39, 1739–1745.

Rangaswamy, N.V., Hood, D.C., Frishman, L.J., 2003. Regional variations in local contributions to the primate photopic flash ERG: revealed using the slow-sequence mfERG. Invest. Ophthalmol. Vis. Sci. 44, 3233–3247.

Rangaswamy, N.V., Frishman, L.J., Dorotheo, E.U., Schiffman, J.S., Bahrani, H.M., Tang, R.A., 2004. Photopic ERGs in patients with optic neuropathies: comparison with primate ERGs after pharmacologic blockade of inner retina. Invest. Ophthalmol. Vis. Sci. 45, 3827–3837.

Rangaswamy, N.V., Shirato, S., Kaneko, M., Digby, B.I., Robson, J.G., Frishman, L.J., 2007. Effects of spectral characteristics of Ganzfeld stimuli on the photopic negative response (PhNR) of the ERG. Invest. Ophthalmol. Vis. Sci. 48, 4818–4828.

Rangaswamy, N.V., Zhou, W., Harwerth, R.S., Frishman, L.J., 2006. Effect of experimental glaucoma in primates on oscillatory potentials of the slow-sequence mfERG. Invest. Ophthalmol. Vis. Sci. 47, 753–767.

Silveira, L.C., Picanço-Diniz, C.W., Sampaio, L.F., Oswaldo-Cruz, E., 1989. Retinal ganglion cell distribution in the cebus monkey: a comparison with the cortical magnification factors. Vision Res. 29, 1471–1483.

Silveira, L.C., Perry, V.H., Yamada, E.S., 1993. The retinal ganglion cell distribution and the representation of the visual field in area 17 of the owl monkey, *Aotus trivirgatus*. Vis. Neurosci. 10, 887–897.

Ueno, S., Kondo, M., Niwa, Y., Terasaki, H., Miyake, Y., 2004. Luminance dependence of neural components that underlies the primate photopic electroretinogram. Invest. Ophthalmol. Vis. Sci. 45, 1033–1040.

Ueno, S., Kondo, M., Ueno, M., Miyata, K., Terasaki, H., Miyake, Y., 2006. Contribution of retinal neurons to d-wave of primate photopic electroretinograms. Vision Res. 46, 658–664.

Viswanathan, S., Frishman, L.J., Robson, J.G., Harwerth, R.S., Smith III, E.L., 1999. The photopic negative response of the macaque electroretinogram: reduction by experimental glaucoma. Invest. Ophthalmol. Vis. Sci. 40, 1124–1136.

Viswanathan, S., Frishman, L.J., Robson, J.G., 2000. The uniform field and pattern ERG in macaques with experimental glaucoma: removal of spiking activity. Invest. Ophthalmol. Vis. Sci. 41, 2797–2810.

Viswanathan, S., Frishman, L.J., Robson, J.G., Walters, J.W., 2001. The photopic negative response of the flash electroretinogram in primary open angle glaucoma. Invest. Ophthalmol. Vis. Sci. 42, 514–522.

Wu, S., Sutter, E.E., 1995. A topographic study of oscillatory potentials in man. Vis. Neurosci. 12, 1013–1025.

Yoshii, M., Päärmann, A., 1989. Hemiretinal stimuli elicit different amplitudes in the pattern electroretinogram. Doc. Ophthalmol. 72, 21–30.

Zhou, W., Rangaswamy, N., Ktonas, P., Frishman, L.J., 2007. Oscillatory potentials of the slow-sequence multifocal ERG in primates extracted using the Matching Pursuit method. Vision Res. 47, 2021–2036.

Twenty-three Gauge Cannula System with Microvitreoretinal Blade Trocar

Makoto Inoue, Kei Shinoda and Akito Hirakata

Br J Ophthalmol published online October 14, 2009
doi: 10.1136/bjo.2009.166207